Development of Bionanocomposite Packaging Film from Carboxymethyl Cellulose, Vanillin and Montmorillonite Nanoclay: Optimization Using Response Surface Methodology

David Jaucian Alcarde Jr, CPP

Abstract

Substituting petroleum-based plastics with biobased or biodegradable alternatives contributes to mitigating the environmental burden of conventional packaging. This project aims to develop and characterize a novel bionanocomposite packaging film made from carboxymethyl cellulose (CMC), vanillin, and montmorillonite nanoclay. A design of experiments approach using Response Surface Methodology was used to investigate compositions in an attempt to optimize the formulation. Samples were manufactured via solvent casting and tested for mechanical properties and oxygen transmission rate (OTR). The microstructure of a selected samples was analyzed using transmission electron microscopy (TEM) to examine the morphology of the nanoclay. Prototype films were successfully produced with overall good mechanical properties and high transparency. Preliminary microstructure analysis vie TEM suggested an intercalated nanoclay structure. The RSM model did not show statistical significance or predictability. This may be due to uncontrolled factors and the small range between the levels. Most of the OTR values, between 150 and 1000 cc/m^2 day, can be consider breathable films. Case-ready meat, fish, sausage, fresh produce and vegetables, and other food goods needing breathable films can be wrapped with these blended compositions, which offer films and/or film structures with a mix of oxygen breathability, high formability, and structural strength.

Introduction

Despite being widely used in all facets of human existence as sophisticated materials, synthetic polymers, fibers, and composites significantly influence the environment, society, and economy. Global production of synthetic polymers and petroleum-based plastic is 400 million metric tons annually [1] and about 500 billion plastic bags are used worldwide at a rate of one million bags per minute

Rochester Institute of Technology
Dusty Rhodes Graduate Student Paper

[2]. Of the plastic garbage generated, only around 10% is recycled, 14% is burned, and the rest 76% is dumped in landfills or ends up in water bodies [3] where it can linger for up to 1200 years [4]. One major issue that necessitates quick thought and innovation in the feedstock material industry is petroleum-based polymers' growing pollution of the world's inland and coastal waterways. Approximately 0.5% of the 350 million tons of annual plastic waste produced worldwide wind up along the coast and in the center of the oceans [5]. The poor degradability of these materials has caused irreparable damage to ecosystems. Recently, there have been studies about micro- and nano-plastic particles that emerge as a hazard to the environment and public health when plastic waste is broken up by natural cause or deteriorated by ultraviolet (UV) rays [6] – [12]. There are also reports of drinking water, food, air samples, and inaccessible places like the Antarctic region that have all been found to have these particles [13]. Thus, increased interest in the study and creation of safer, more circular, and functional green materials has resulted from several factors, including the growing potential and initiative for low-cost resources and energy-efficient renewable bio-based solutions, stricter legal requirements and more stringent trade policies, consumer demand for eco-friendly processes and products, carbon-neutral programs and technologies, and the sustainable solutions that continue to evolve [14]. Commercial exploitation of naturally occurring minerals and abundant natural polymers like cellulose has been developed to strengthen the competitive position of the bio-based and bio-nanocomposites industry and supplement or replace society's reliance on plastics and polymers derived from fossil oil. Cellulose generated from plants is the world's most prevalent biopolymer while clay minerals are equally abundant at the earth's surface. These materials have been the subject of scientific investigations for potential commercial and medicinal applications [15] – [24].

This project aims to develop and characterize a novel bionanocomposite packaging film made from carboxymethyl cellulose (CMC), vanillin, and montmorillonite nanoclay. CMC is a derivative of naturally occurring cellulose that is usually sourced from wood pulps and cotton lint. Vanillin is an aldehyde of phenol, also of plant origin and it has a wide array of applications in the food, beverages and the pharmaceuticals industry [25]. A montmorillonite (MMT), on the other hand, is a nontoxic silicate clay that is abundant in the environment and has seen its promising potential as reinforcement material for biofilms like chitosan film [26]. Since the materials from which the packaging film is made are environment-friendly, sustainable, and none of these materials have been confirmed and reported to have posed threat to human health, the packaging film can find application in the food industry as a potential replacement for synthetic plastic films and bags for food. The addition of vanillin and montmorillonite nanoclay may be instrumental in developing a packaging film with enhanced properties since previous studies have shown that incorporating these materials were observed to have significant improvements in a biobased film's physical properties like water vapor permeability, tensile strength and rigidity [27] – [29].

Several studies on these sustainable materials have been published with the purpose of developing novel bioplastic film or bio-based material that has a potential viability to replace synthetic plastic for packaging application, but very few of these studies have attempted to statistically determine the optimum formulation to yield either the maximum desirable property or the minimum undesirable attributes. In the work of Mohammadi et al. [30], a nanocomposite packaging film was developed from CMC, Okra Mucilage (OM), and Zinc Oxide nanoparticles (ZnO-np) with some notable observations of antibacterial activity on the samples incorporated with OM. Ahmad et al. [31], Eshagi et al.[32] and Singh et al. [33] are independently performed, but similar studies have shown success in developing CMC nanocomposite film that used active compounds to extend the shelf lives of certain food products. However, their works failed to examine the optimal formulation ratio of the materials that could maximize at least one of the specific properties of the resultant film.

This project aims to implement Response Surface Methodology (RSM) in the investigation and optimization of CMC-vanillin-nanoclay packaging film. RSM is a statistical tool and an experimental design technique that may be used to optimize responses and is helpful for modeling and analyzing situations where multiple variables affect the response [34]. Some of the previous studies where RSM has been successfully implemented have been shown to have utilized at least one of the physical properties as the objective response for bio-based and bionanocomposite films [35] – [39]. However, there has rarely been a published report of RSM's application on CMC-vanillin-MMT nanoclay film.

Literature Review

Bionanocomposite

Bionanocomposites are materials that combine inorganic solids with biopolymers, with at least one dimension on the nanoscale [40],[41]. The word "bionanocomposite," also known as "green composites," "biohybrids," or nanobiocomposites (NCs), was initially used in 2004 [42], and because they exhibit multidimensional properties like biodegradability, biocompatibility, antimicrobial, sensing ability, optical, mechanical, and gas barrier properties, bionanocomposites are fast becoming an emerging field of study for both polymer scientists and nanotechnologists [43]. Bionanocomposites have highly peculiar characteristics that set them apart from their microscale equivalents. Edible and biodegradable materials can find greater applications because of these inorganic-organic hybrid. Because of their hydrophilic nature, biopolymers have low water vapor permeability; on the other hand, bionanocomposites exhibit excellent water vapor permeability because of their maze-like structure, which creates a winding path for various molecules like gases, water, oxygen, etc. thus enhances their

permeation rates. When compared to parent polymers, the barrier qualities of bionanocomposites can be improved by up to 50% [44][45].

Because of the properties that come from combining biopolymers and nanoparticles, the creation of bionanocomposites is currently in the spotlight [46]. Its versatility and functionality can be observed from recent research on smart or intelligent packaging where bionanomaterials were developed incorporating active and bioactive components that aimed at extending the products' shelf lives, improving the quality and safety, providing detailed information, and warning about possible spoilage and problems [43]. Bionanocomposites have also been used in biomedical science like in wound dressing, drug delivery, anti-cancer treatments, and tissue engineering [47][48][42][49][50]; in fungal disease management [51]; in wastewater treatment [52][53]; and recently, in energy storage applications [54].

Carboxymethyl Cellulose

The CMC is the primary and most important cellulose derivative [55]. Formed by introducing the carboxymethyl group into the cellulose structure, CMC is water-soluble and is known to be more beneficial than its parent form [56]. This cellulose-derived chemical is created when cellulose reacts with monochloroacetic acid, causing carboxymethyl groups to replace the hydroxyl groups in the glucose residues at carbon numbers 2, 3, and 6, with carbon number 2 substitution being somewhat more noticeable [55]. Connecting the repeated units are ~-1,4-glycosidic linkages. Only a few anionic carboxymethyl (i.e., $-CH_2COOH$) groups in the CMC structure take the place of the hydrogen atoms from certain hydroxyl groups found in the pristine cellulose infrastructure, which is the primary molecular difference between CMC and cellulose [57].

CMCs can be synthesized from different sources, including those coming from plant-based precursor materials like agricultural by-products and wastes, and non-conventional precursors like waste materials of textile factories (e.g., cotton linter, knitted rags) and also used office and household products like paper sludge, paper waste, and used papers-based materials. In other parts of the world, plant-derived materials are more readily available at a very low price, sometimes even free, compared to wood as the commercial antecedents of CMC. Examples of plant-based precursors that are considered agricultural wastes are rice husks [58], asparagus stalks [59], corn cobs [60], corn stalks [61], corn husks [62], sago palm [63], banana rachis [64], banana stem [65], orange peelings [66], pineapple peelings [67], sugarcane bagasse [68], and bark of a durian tree [69]. Non-conventional precursors, on the other hand, include paper sludge [70], office paper waste [71], knitted rags [72], waste from the textile industry [73], cotton gin waste [74], and waste cotton linter [75].

CMC and other materials derived from it have found a wide array of applications in the fields of biomedical science/engineering, pharmaceuticals industry, textile manufacturing, construction materials, food engineering, polymer science and plastics engineering, cosmetics, paper, and oil industries due to their simple, inexpensive process of synthesis, an abundance of the sources of raw materials, distinctive surface attributes [76], [77], tensile strength and other mechanical properties [78], differences in moldability and flexibility [79],[80], hydrophilicity [81], [82], viscosity [83], and countless other factors. For example, CMC, its derivative, and composites are widely used in biomedical science and engineering for diagnosing different diseases [84], for the design and fabrication of 3D scaffolds for bio-implants [85], tissue engineering [86], bone-tissue reconstruction, wound dressing [87], non-woven fabrics [82], and artificial organs or mimics of extracellular polymeric layers [88].

Many researchers in the last decade have gained interest in developing composite packaging materials mostly in the form of films that have used CMC for specific food applications. These packaging films vary in composition and purpose. For example, one of the films developed claimed to be a biodegradable and eco-friendly hydrogel film and is composed of polyvinylpyrrolidone (PVP) and CMC that was intended as a primary packaging material for food [89]. An essential oil doped CMC/chitosan/montmorillonite active nanocomposite film was developed that was reported to have extended the shelf life of camel meat [90], while a metal cation doped CMC/Polyvinyl alcohol (PVA)/zeolite packaging film was reported to have shown biodegradability and antimicrobial property that can prevent early spoilage of food [91]. More recent packaging innovations involves the incorporation of plant pigments like anthocyanin into CMC matrix, forming a pH-sensitive packaging film that can intelligently monitor the freshness and quality of food [92].

Vanillin

Vanillin, also known as 4-hydroxy-3-methoxybenzaldehyde, is a crystalline powder that ranges in color from white to faintly yellow. It has a unique, sweet scent and is soluble in water at ambient temperature but soluble in boiling water. Its primary functional groups are classified as aldehyde, hydroxyl, and ether in its chemical composition. Hydroxyl and ether together constitute the core vanillyl (4-hydroxy-3-methoxybenzyl) group while several bioactive substances known as vanilloids, such as vanillylmandelic acid, capsaicin, zingerone, gingerol, vanillic acid, and eugenol, are also part of this vanillyl backbone [93]. Although other plants, including commercial goods like tobacco, do contain trace levels of vanillin [94], the pods of the Vanilla orchid continue to be the only commercial source of natural vanillin [95]. The annual production of natural vanillin is approximately 7500 tons, depending on the origin and the environment [96]. The annual output of natural vanillin is significantly lower than the increasing market

demand for it (millions of tons) [97][98]. Consequently, vanillin is nowadays manufactured chemically to substitute natural vanillin in order to satisfy the expanding demand for it in the global market [96]. There was an estimate of 18,600 tons of vanillin in the world in 2016, and from 2017 to 2025, there will be an annual growth of 6.2% in the demand for vanillin. An estimated 724.5 million USD will be the global market share of vanillin by 2025 [99][100].

In the food and beverage sectors, vanillin is a flavor and biological preservative that is frequently utilized. It is frequently used as a pharmaceutical intermediary in the production of several medications, including levodopa, papaverine, and dopamine. It is also used as a defoaming agent in some sectors, a scent in cosmetics and fragrances, and a growth-promoting agent in agriculture [97][101][102]. One study showed that when combined with carrageenan, vanillin forms a composite hydrogel that has been shown to be effective in wastewater treatment [103].

Vanillin, as an intermediate, has been demonstrated in recent research to have significant applications in material science and biomedical engineering, including wound dressings, anti-tumor medications, drug delivery systems, and battery energy storage [104]. A Schiff base bond can be formed between the amino groups of chitosan molecules and the aldehyde group of vanillin.
Vanillin also demonstrates notable biocompatibility and antimicrobial action. As a result, scientists are interested in vanillin as a cross-linking agent [105]. Dressings based on hydrogels now contain vanillin. When self-healing hydrogels are used instead of conventional dressings like gauze, absorbent cotton, and bandages, they have a higher potential for wound healing and improved antibacterial activity [106]. Researchers have created a composite hydrogel with outstanding bactericidal efficacy against pathogenic bacteria, including Escherichia coli and Staphylococcus aureus, by combining lysine, polyvinyl alcohol, and vanillin. By the seventh day, the composite-treated wounds had regenerating epidermis, covering 95–100% of their surface areas [107]. In packaging research, vanillin finds its used as a natural cross-linking agent for biopolymers [25][28][37][108][109] in the development of composites or nanocomposites. The compound also plays an important role in the valorizing of agricultural wastes [110] – [112] wherein low-value residues like bagasse, plant stalks, cobs, peelings, straws, and non-food seeds are being processed to convert these materials into products that are of higher or significant value or recover and generate value-added products.

Nanoclay and Montmorillonite

Clays are extremely important industrial materials with hundreds of documented applications and a remarkably wide array of properties and uses primarily because of their mineral structure and composition [113]. Clay's structure can exist in

tetrahedral or octahedral sheets [114], and this clay structure and composition largely dictate their properties and applications. Clays are used in numerous diverse fields, including engineering, environmental remediation, geology, agriculture, building and infrastructure, and processing industries [113]. Because of their strength and high thermal conductivity, clays are also employed in ceramic plants as the principal raw material [115]. These minerals are sometimes modified by turning them into nanoclay and mixing them with polymers to develop packaging films with enhanced gas barriers and mechanical properties for use as food packaging materials [116]. When silicate nanoparticles are assembled into a layered structure, the resulting minerals are called nanoclays [117]. Depending on the type of silicate, each layer can be approximately 1nm in thickness, with lateral dimensions ranging from 300 Å to several microns [118]. When these nanoclays are integrated into polymers, the reinforcement is developed and may be responsible for their high aspect ratio (length/thickness) as well as their intercalation and exfoliation properties [119]. The structure of a nanocomposite can either be exfoliated or intercalated [120], and the former is obtained when the silicate layers are uniformly diffused within the polymer matrix. Besides having an exfoliated structure, nanocomposites can also be intercalated [116]. When the extended polymer chains intercalate between the silicate layers, an intercalated nanocomposite is produced, which has an alternating pattern of polymeric and inorganic layer structure and a highly organized multilayer morphology. Exfoliated nanocomposites generally exceed the mechanical performance of intercalated nanocomposites [121].

Nanoclays are one of the classes of nanomaterials that have been recently employed in the food and packaging industries that contribute to an increase in food safety, food quality and delivery of bioactive compounds [122]. These nanomaterials are incorporated into polymer matrices for the purpose of enhancing the film properties, and the product, known as nanocomposites, could be able to develop these improved properties because of the synergistic bond between the polymeric matrix and the nanomaterials [123]. Because it comes from a natural source and is suitable for use in packaging applications, clay, in the form of nanoclay, is one of the most popular nanomaterials for food packaging applications. Nanoclays are frequently employed in the production of packaging films with excellent barrier and thermal durability, as well as biodegradable films and coatings, because of their low cost, biocompatibility, and availability [116]. These nanoclays are mineral silicates with multiple layers, and they stack on top of one another to form a clay crystallite structure [124]. Van der Waal's force and electrostatic interactions hold these layers together in parallel, and they are composed mainly of metal oxides, alkali metals, trace amounts of organic matter, iron, magnesium, alkaline earth metals, and other cations [125].

When appropriately mixed in the polymer matrix, the nanoclays become highly exfoliated. This exfoliation enhances the bond between the polymer matrix and

the nanoclays, consequently improving the mechanical properties of the resultant nanocomposites [126].

Nanoclays like the montmorillonite (MMT) nanoclay has a broad range of applications in human health, particularly in drug delivery systems [127][128], tissue engineering [129], bone regeneration [130], and antimicrobial treatments [131][132]. MMT nanoclay, while showing promise in various health applications, also raises several controversies and concerns in human health due to potential risks and challenges [133] [134]. Research has revealed that most of the toxic effects of clay minerals are caused by inhalation [133][134][135]. Since clay minerals like MMT may be found in food, medicine, and other items, oral consumption is one of the most likely ways that the public may be exposed to these minerals. Studies have shown that an unmodified MMT has no mutagenic and genotoxic potentials [136], [137] but the ingestion of modified MMT nanoclay at "high" concentrations can lead to gastrointestinal disturbances [127] and has the potential to exhibit cytotoxicity [138], which may affect its suitability for certain medical applications. Despite these potential health risks, the use of hexadecyltrimethylammonium bromide-modified MMT organoclay was approved by the USFDA as a food contact substance [139]. The EFSA Panel on Food Contact Materials, Enzymes, Flavorings, and Processing Aids also recommended the use of dimethyl-alkyl ammonium-modified MMT as additives in polymer blend in sealers for packaging that may come in direct contact with food [140].

Food packaging films and coatings frequently employ nanoclay like montmorillonite (MMT) as a nanofiller [44][141][142][143]. Montmorillonite belongs to a class of clay called smectite [113]. It comprises the edge of an octahedral $Al(OH)_3$ sheet fused with two tetrahedral sheets of silica material. A high surface-to-volume ratio and cation-exchange characteristics characterize the alumino-silicate smectite clay mineral [144]. These characteristics offer sufficient carrying capacity for active chemicals, high miscibility with cationic polymers, and water dispersibility. The addition of MMT significantly improves the water vapor permeability (WVP), mechanical and physical characteristics, and UV blocking properties of biopolymers [145]. In one study, gelatin films with MMT and copper (II) ions were shown to have developed antibacterial properties, and a 5% MMT in the same film enhanced the tensile strength by more than 200% while the water vapor permeability and elongation-at-break were reduced by around 30 and 40% respectively [146]. The enhanced affinity of the biopolymer for MMT and the reduced mobility of the protein chains were credited with improving the tensile strength. Similarly, water vapor transfer through the film matrix is delayed and obstructed by the uniformly distributed impermeable nanoclays. Furthermore, in the copper (II) loaded gelatin-MMT film, the growth of Escherichia coli and Listeria innocua was inhibited due to the bactericidal action of the copper (II) ions. The cations interacted with the surface of the bacterium, increasing the

permeability of the cell membrane and causing cell death, breakdown of the cell wall, and loss of cell content [146]. Nanocomposites of cellulose acetate and MMT have been reported to have promising results [147][148][149][150]. Chitosan/MMT nanocomposites have also been developed [19][23][151][152], and the resultant materials were environment-friendly, and some may have important properties that are comparable to the conventional petroleum-based films. However, nanocomposites of carboxymethyl cellulose (CMC) and MMT have been found to be quite few or limited, and this project filled this gap by developing CMC/Vanillin/MMT nanocomposite film.

Methodology

Materials

Sodium carboxymethyl cellulose (Average MW ~90,000) has been obtained from Sigma-Aldrich (Saint Louis, MO, USA). Vanillin has been obtained from Fluka Analytical (USA). Nanoclay, surface modified Montmorillonite clay has been obtained from Sigma-Aldrich (Saint Louis, MO, USA). Glycerol has been acquired from VWR (Pennsylvania, USA). The procedure in fabricating the film was inspired from the methods of Li et. al. [153], Mohammadi et. al. [30], Jha P. [154], Beigzadeh Ghelejlu et. al. [26], Tomadoni et. al. [109], and Zhang et. al. [155]. The adaptation of more than one method from more than one literature was because the nanocomposite film material developed in this project has unique composite of biomaterials. Solvent casting was used to create the CMC, vanillin, and MMT bionanocomposite films. To make the solution for CMC film, two grams of CMC were dissolved in one gram of glycerol (which accounted for 50% of the total solid weight in solution) in 100 milliliters of distilled water. The mixture was then aggressively mixed for sixty minutes at 50 to 60 degrees Celsius, using a magnetic stirrer set at 700 rpm. Nanoclay suspension was then added to the CMC solution at 1%, 1.5%, and 2% w/w CMC as determined from the experimental design.

Nanoclay (MMT) suspensions with three different concentrations (1, 0.659, 1.5, 2, and 2.341% w/w of CMC) were prepared by dispersing appropriate amounts of MMT in 10 mL of 1% acetic acid solution following 5 hours of ultrasonic mixing. About 5 mL of this solution was mixed with CMC solutions and stirred for 30 minutes. Vanillin was added in different concentrations (3%, 5%, and 7% w/w of CMC) and continued stirring at 700 rpm for 1 hour. The stirring rate was reduced while adjusting the pH to 4.6 with 1-4% acetic acid. Finally, the film solutions were placed into a centrifuge (5000 rpm for 5 mins) to remove bubbles. All the film solutions were cast evenly onto a leveled 12 cm x 12 cm plexiglass plate and then dried for about 48 hours at about 20^0C ambient temperature. The exact amount of each treatment, a constant amount of each treatment, and a constant amount of film-forming solution's weight to plate area of 3:1 (66.9 grams) was

applied for casting onto each plate. The resultant dried film was peeled from the casting surface. All treatments were made unreplicated.

Design of Experiment

This project fabricated bionanocomposite packaging film from biomaterials, including carboxymethyl cellulose (CMC), vanillin, and montmorillonite (MMT) nanoclay as nanofiller. The procedure used glycerol as a constant-weight plasticizer throughout each of the runs. This project implemented Response Surface Methodology (RSM) to investigate and optimize CMC-vanillin-MMT packaging film. The experimental design shown in Table 1 is a Central Composite Design (CCD) with three factors and values are also shown in coded and uncoded units. RSM is a useful statistical tool and experimental design technique when assessing scenarios where several variables influence the response [156]. In the said table, A represents the MMT, B for vanillin, and C for stirring temperature. There have been few, if any, published reports on the development of CMC-vanillin-MMT nanoclay film, more so on the use of RSM to optimize, or at least, to evaluate the effect of each factor on the properties of the said nanocomposite film.

This project addresses the research gap from the study by Li et al. [153] and Mohammadi et al. [30], in which a bionanocomposite film for food packaging applications was developed and characterized. Although the water vapor permeability was analyzed in their studies, they failed to examine the effect of the incorporation of filler nanoparticles on the oxygen permeation, and no attempt was made, preliminary or otherwise, to optimize the blend. These gas permeabilities (oxygen, water vapor, etc.) are factors that also critically determine the shelf life of food products. This study also aims to fill the research void that can be observed in the study by Zahedi et al. [157], in which a hybrid material between MMT and ZnO nanoparticles was first developed, followed by utilizing this newly formed material to improve some of the properties of CMC. This innovation may look scientifically bright and sound. Still, a closer analysis may find that the fabrication method introduced more process cost and complexity by incurring several processing steps to develop a material whose properties may be comparable to the product, requiring simplified procedures and fewer materials.

		coded			uncoded			
StdOrder	RunOrder	A	B	C	A	B	C	Response
1	17	-1	-1	-1	1%	3%	50 ^{0}C	y1
2	16	1	-1	-1	2%	3%	50 ^{0}C	y2
3	7	-1	1	-1	1%	7%	50 ^{0}C	y3
4	5	1	1	-1	2%	7%	50 ^{0}C	y4
5	12	-1	-1	1	1%	3%	60 ^{0}C	y5
6	13	1	-1	1	2%	3%	60 ^{0}C	y6
7	10	-1	1	1	1%	7%	60 ^{0}C	y7
8	8	1	1	1	2%	7%	60 ^{0}C	y8
9	3	-1.68179	0	0	0.659%	5%	60 ^{0}C	y9
10	14	1.681793	0	0	0.234%	5%	55 ^{0}C	y10
11	6	0	-1.68179	0	1.5%	1.636%	55 ^{0}C	y11
12	11	0	1.681793	0	1.5%	8.364%	55 ^{0}C	y12
13	2	0	0	-1.68179	1.5%	5%	46.591 ^{0}C	y13
14	1	0	0	1.681793	1.5%	5%	63.409 ^{0}C	y14
15	15	0	0	0	1.5%	5%	55 ^{0}C	y15
16	9	0	0	0	1.5%	5%	55 ^{0}C	y16
17	4	0	0	0	1.5%	5%	55 ^{0}C	y17
18	19	0	0	0	1.5%	5%	55 ^{0}C	y18
19	18	0	0	0	1.5%	5%	55 ^{0}C	y19

Table 1: DOE and sample preparation order

To determine their mechanical characteristics, the developed film samples will be put through a series of mechanical and physical testing. A piece of equipment called the OpTech-O_2 Model P oxygen permeation machine (OPM) will be used to measure the oxygen permeation rates in the film, while the universal testing machine (UTM) can be used to assess the tensile strength, modulus, and elongation at break (EAB). The former is compliant with ASTM F2714-08, while the latter can be configured to comply with ASTM D882-18.

Sample Preparation for Tensile Strength Test

The test specimens were made up of uniformly sized, thick strips that were at least 50 mm longer than the distance between the grips that were being used. The specimens' nominal width was 5.0 mm at the very least and 25.4 mm at the very most. At least an 8-fold width-thickness ratio was employed. A cutting jig was used to cut specimens with the utmost care, preventing microscopic tears and nicks that might lead to premature failures. This made sure that along the specimen's length between the grips, the edges were parallel to within 5% of its breadth. To ensure that the specimens were free of defects related to sample preparation, no microscopic inspections of the samples were carried out. Test specimens were chosen so that, for specimens with a thickness of less than 0.25 mm, the thicknesses were uniform within 10% of the average thickness over the specimen's length between the grips, and within 5% for specimens with a

thickness greater than 0.25 mm but less than 1.00 mm. Variabilities in thickness outside of these limits were not tested. As per ASTM D618 method A, test specimens were conditioned for at least 40 hours at 23 ± 20C and 50 ± 10% relative humidity before the test.

Transmission Electron Microscopy (TEM)

Transmission electron microscopy (TEM) is a powerful imaging technique used in material science and biology to investigate the structure and properties of materials at the atomic or molecular scale. This method is particularly useful in characterizing thin film samples and other nanoscale materials. TEM uses a focused electron beam that transmits through a thin specimen to produce images of high resolution, allowing researchers to observe fine details of the internal structure of the sample [158]. The basic principle of TEM involves the interaction between a high-energy electron beam and a thin specimen. As the electrons pass through the sample, they interact with the atoms in the material, scattering in various directions. The unscattered or slightly scattered electrons form an image as they hit a fluorescent screen or a digital detector [159]. This imaging allows for visualization at atomic-level resolution, revealing structural features such as lattice arrangements, defects, and grain boundaries. To obtain the best results from TEM analysis, it is critical to prepare thin and uniform samples. For thin film samples, the preparation process generally involves the following steps: Substrate Preparation: The film samples are often deposited on a substrate (e.g., silicon, glass) to ensure they are thin and uniform. Sample Cutting and Mounting: A small piece of the thin film is cut from the substrate and mounted onto a TEM grid [160]. The grid serves as a support for the thin film and must be thin enough to allow electron transmission. Thinning the Sample: To enable electron transmission through the sample, the thin film must be further thinned to an appropriate thickness, typically less than 100 nm. This is achieved using methods such as ion milling, which utilizes a focused ion beam to remove excess material [158]. Polishing and Cleaning: The sample is carefully polished to remove surface imperfections and ensure uniform thickness. It is then cleaned to remove any debris or contaminants that may interfere with the electron beam. Storage: Once prepared, the samples are typically stored in a vacuum environment or under controlled atmospheric conditions to prevent degradation [158]. After preparation, the sample is placed in the TEM, and imaging is performed by transmitting the electron beam through the sample and capturing the transmitted electrons with a detector.

Results and Discussion

Mechanical Testing

Table 2 presents the mechanical properties like the average tensile strength (TS), percent elongation at break (EAB), and modulus of elasticity (MOD) of samples of CMC/Vanillin/MMT film of varying component concentrations. As can be seen in the table, the bionanocomposite film sample containing 1.5% MMT nanoclay, 5% vanillin, and 55^0C mixing temperature showed the highest tensile strength, and this data point represents one of the center points of the rotatable central composite design (CCD) of the experiment. It can also be observed in the table that another center point recorded the highest elongation, while a sample consisting of 2% MMT nanoclay and 3% vanillin mixed at 60^0C exhibited the highest modulus of elasticity. It is noteworthy to emphasize that the factorial and axial points of the experimental design were unreplicated and that only the center points were replicated five times to estimate the curvature of the model. From Table 2, it can be observed that there were only four data points that represent the center points, indicating that one of the test runs was damaged due to uncontrollable factors.

No.	Sample	Code	Tensile Strength (MPa)	Modulus of Elasticity (Mpa)	Elongation at Break (%)
1	1%MMT/3%Vanillin/Temp-50C	MT01VA3T50	17.4 ± 5.8	537.00 ± 177.38	27 ± 16
2	1%MMT/3%Vanillin/Temp-60C	MT01VA3T60	11.1 ± 4.7	208.54 ± 209.42	44 ± 16
3	1%MMT/7%Vanillin/Temp-50C	MT01VA7T50	14.1 ± 3.6	381.28 ± 248.89	28 ± 13
4	1%MMT/7%Vanillin/Temp-60C	MT01VA7T60	16.1 ± 5.8	625.92 ± 345.13	23 ± 7
5	2%MMT/3%Vanillin/Temp-50C	MT02VA3T50	12.7 ± 2.8	398.14 ± 132.46	21 ± 8
6	2%MMT/3%Vanillin/Temp-60C	MT02VA3T60	17.0 ± 2.4	742.64 ± 171.61	18 ± 9
7	2%MMT/7%Vanillin/Temp-50C	MT02VA7T50	13.1 ± 2.7	449.18 ± 109.06	24 ± 3
8	2%MMT/7%Vanillin/Temp-60C	MT02VA7T60	15.5 ± 2.7	640.34 ± 266.17	17 ± 14
9	1.5%MMT/5%Vanillin/Temp-55C	MT15VA5T55-1	11.5 ± 4.5	248.27 ± 154.45	39 ± 10
10	1.5%MMT/5%Vanillin/Temp-55C	MT15VA5T55-2	19.9 ± 3.7	628.54 ± 96.96	17 ± 7
11	1.5%MMT/5%Vanillin/Temp-55C	MT15VA5T55-3	14.7 ± 1.8	443.98 ± 82.41	31 ± 14
12	1.5%MMT/5%Vanillin/Temp-55C	MT15VA5T55-4	17.0 ± 6.6	591.78 ± 268.03	27 ± 9
13	1%MMT/3%Vanillin/Temp-46.59C	MT15VA5T4659	11.7 ± 1.7	401.52 ± 40.56	21 ± 10
14	1.5%MMT/5%Vanillin/Temp-63.40C	MT15VA5T6340	12.7 ± 2.4	372.37 ± 35.84	25 ± 8
15	1.5%MMT/1.63%Vanillin/Temp-55C	MT15VA163T55	16.5 ± 2.9	684.32 ± 190.08	17 ± 4
16	1.5%MMT/8.36%Vanillin/Temp-55C	MT15VA836T55	14.7 ± 2.8	577.18 ± 241.55	27 ± 6
17	2.34%MMT/5%Vanillin/Temp-55C	MT234VA5T55	16.6 ± 3.3	492.41 ± 37.07	34 ± 12
18	0.659%MMT/5%Vanillin/Temp-55C	MT0659VA5T55	12.2 ± 2.8	370.46 ± 96.41	27 ± 18

Table 2: Mechanical test results of CMC/Vanillin/MMT Nanoclay

The mechanical properties of the bionanocomposite films containing carboxymethyl cellulose, vanillin, and montmorillonite nanoclay are presented in the table above, indicating a variation in tensile strength, modulus of elasticity, and elongation at break across different formulations. These results demonstrated how changes in composition (vanillin and montmorillonite content) and processing conditions (temperature) can impact the mechanical performance of the films. Figure 1 depicts the average tensile strength of the bionanocomposite

film samples. The figure has shown that the tensile strength of the samples varies significantly, ranging from 11.1 MPa to 19.9 MPa. For example, sample MT01VA3T50 with 1% MMT and 3% vanillin exhibited a tensile strength of 17.4 MPa, while the similar formulation at a higher temperature (MT01VA3T60) showed a decrease to 11.1 MPa. The sample MT15VA5T55-2 with 1.5% MMT and 5% vanillin displayed the highest tensile strength at 19.9 MPa, suggesting the combination of moderate MMT and vanillin content, along with processing at 55°C, might be beneficial for enhancing tensile strength. In general, the results suggest a potential trend of higher MMT content (1.5-2.34%) and optimal vanillin levels (5%) leading to better tensile strength.

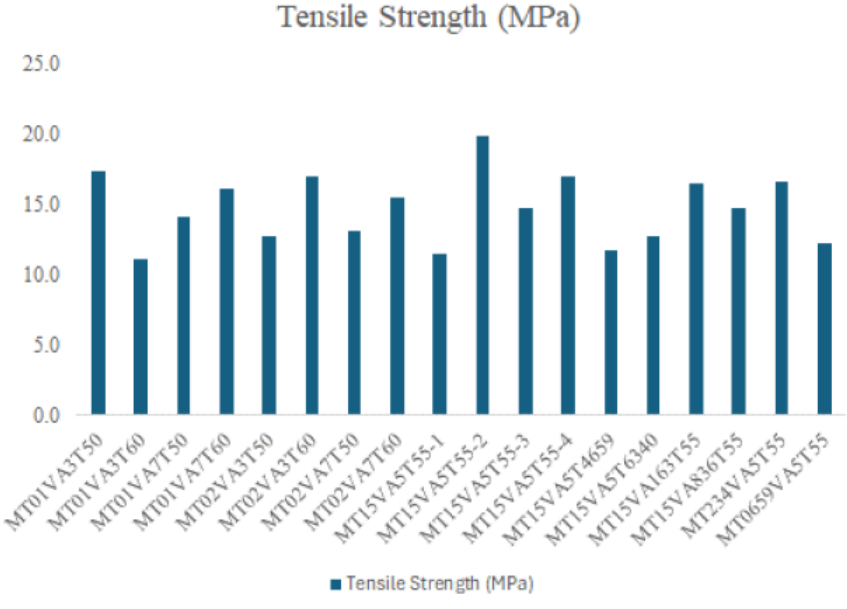

Figure 1: Tensile strength of samples

Film sample	Tensile strength (Mpa)	Reference
CMC/Vanillin/MMT	**11.1 - 19.9**	**Alcarde, D. (RIT, 2024) - unpublished article/project**
PLA/PCL/TPS	14.11 - 17.73	Wang, R. (2018) - RIT Masters thesis
PLA/PCL/TPS/Vanillin	11.86 - 13.86	Wang, R. (2018) - RIT Masters thesis
CMC/Starch/MMT	9.83 - 27.55	Ghanbarzadeh, B. et. al. (2014)
PVA/CMC/Starch/MMT	18.36 -20.38	Taghizadeh, M. et. al. (2013)
CMC/MMT	17 - 39	Gutierrez, M. et. al. (2012)
CMC/Starch	6.57 - 16.11	Ghanbarzadeh, B. et. al. (2010)
CMC/Starch/MMT	9.83 - 27.55	Almasi, H. (2010)
CMC/Oleic acid	2.23 - 17.77	Ghanbarzadeh, B. and Almasi, H. (2011)
CMC/ZnO	5.1 - 6.4	Kanmani, P. and Rhim, J. (2014)
CMC/Ag	3.9 - 8.8	de Moura, M. (2013)
CS/MMT	0.2 - 1.2	Wilpiszewska, K. et. al (2015)
CA/PEO/ZnO	2.44 - 3.60	Pittarate, C. et. al. (2011)
Chitosan/ZnO	0.003 - 0.021	Das, K. et. al. (2014)
Starch/ZnO/CMC	3.94 - 9.81	Yu, J. et. al. (2009)
Starch/TiO_2/MMT	4.86 - 5.24	Oleyaei, S., Almasi, H., Ghanbarzadeh, B., and Moayedi, A. (2016)
Starch/TiO_2	2.66 - 3.56	Oleyaei, S., Zahedi, Y., Ghanbarzadeh, B., and Moayedi, A. (2016)

Table 3: Tensile strength of CMC-based nanocomposite films compared with some film composites.

Table 3 lists the tensile strengths of some composites and CMC-based composites. As shown in this table, the tensile strength range of the CMC/Vanillin/MMT nanocomposite film is between 11.1 and 19.9 MPa. This places the film towards the higher end of the range in terms of tensile strength compared to other composite films listed in the table. PLA/PCL/TPS composite shows a similar range of tensile strength from 14.11 to 17.73 MPa, which slightly overlaps with the lower end of the CMC/Vanillin/MMT range. However, the range of the latter is broader.

PLA/PCL/TPS/Vanillin composite has a tensile strength range of 11.86 to 13.86 MPa, which is on the lower end of the CMC/Vanillin/MMT range, suggesting that CMC/Vanillin/MMT might be a stronger option compared to the addition of vanillin to PLA/PCL/TPS. CMC/Starch/MMT ranges from 9.83 to 27.55 MPa, covering a broader spectrum. Although its upper end is higher than the CMC/Vanillin/MMT composite, it starts much lower, suggesting a higher variation and less consistency in performance. PVA/CMC/Starch/MMT composite film has a tensile strength range of 18.36 to 20.38 MPa, closely aligning with the upper end of the CMC/Vanillin/MMT range, indicating a similar tensile strength potential but a narrower range. CMC/MMT composite ranges from 17 to 39 MPa, showcasing the highest potential tensile strength in the list. This indicates that pure CMC with MMT reinforcement can offer higher tensile strength, but the range is broad.

CMC/Starch composite's tensile strength is between 6.57 and 16.11 MPa, starting much lower than the CMC/Vanillin/MMT and indicating potentially inferior performance. Other composites like CMC/Oleic acid, CMC/ZnO, CMC/Ag, CS/MMT, CA/PEO/ZnO, Chitosan/ZnO, Starch/ZnO/CMC, Starch/TiO_2/MMT, and Starch/TiO_2 all have lower tensile strength ranges, suggesting they might not be as suitable as the CMC/Vanillin/MMT for applications requiring higher tensile

strength. The CMC/Vanillin/MMT composite film generally shows a good balance of tensile strength compared to most other composites listed. Its tensile strength range is comparable to some of the other stronger composites, making it a potentially suitable material for applications where moderate to high tensile strength is desired.

Figure 2 shows the modulus of elasticity of the CMC/Vanillin/MMT nanoclay sample. As shown the figure, the modulus of elasticity also varied across the samples, ranging from 208.54 MPa to 742.64 MPa. A higher modulus typically indicates a stiffer material. For instance, sample MT02VA3T60, which contains 2% MMT and 3% vanillin processed at 60°C, displayed the highest modulus of elasticity at 742.64 MPa. In contrast, the similar formulation processed at 50°C (MT02VA3T50) showed a significantly lower modulus of elasticity at 398.14 MPa, indicating a potential sensitivity to processing temperature in terms of stiffness.

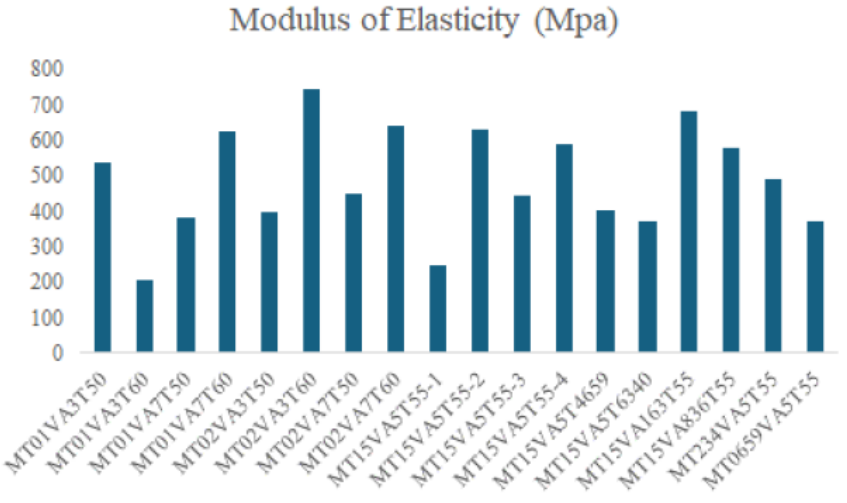

Figure 2: Modulus of elasticity of samples

Figure 3 shows the elongation at break of the CMC/Vanillin/MMT nanoclay sample. As shown the figure, elongation at break percentages vary widely across the samples, ranging from 17% to 44%. Samples with a higher vanillin content generally exhibited higher elongation at break. For instance, samples MT15VA5T55-1 and MT01VA3T60 with higher vanillin content (5% and 3%, respectively) demonstrated elongation at break of 39% and 44%, respectively. This suggests that higher vanillin content may improve the film's flexibility and ability to stretch before breaking. As can be observed from the figures depicting the mechanical test results of, there is no definite trend that can immediately be

seen which is typical in any of the RSM designs since the components are not organized in either increasing or decreasing levels.

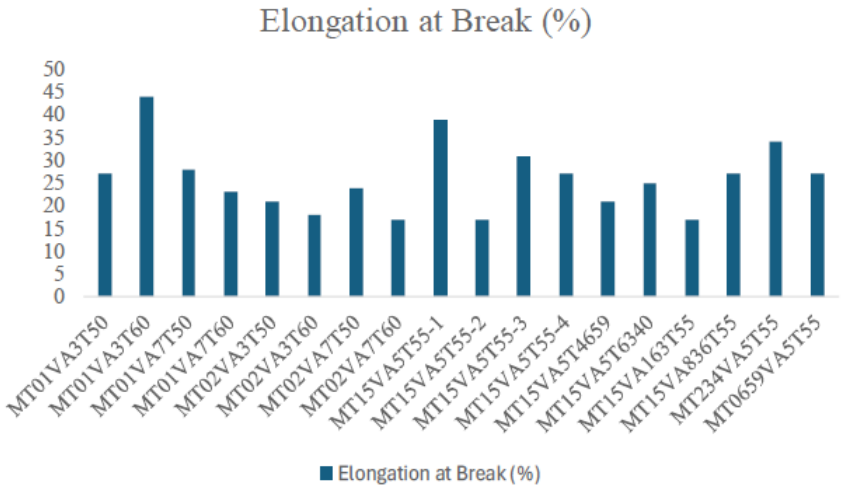

Figure 3: Percent elongation of samples

Oxygen Permeation Test

Table 4 tabulates the data representing the oxygen transmission rate (OTR) of different samples in a three-factor, two-level central composite design (CCD) study. The three factors under consideration are the montmorillonite (MMT) concentration with the levels tested include 0.659%, 1%, 1.5%, 2%, and 2.34%. Another factor used was the vanillin concentration with the levels tested include 0.836%, 1.63%, 3%, 5%, and 7%, and lastly, the mixing temperature with the levels tested include 46.5°C, 50°C, 55°C, 60°C, and 63.4°C. The measured response in the study is the oxygen transmission rate, which is expressed in cc/m^2-day. In can be observed that as the temperature increases, the oxygen transmission rate tends to increase. For instance, when comparing samples with 1% MMT and 3% vanillin at 50°C and 60°C (samples MT01VA3T50 and MT01VA3T60), the OTR increases significantly from 283.52 cc/m^2-day to 2248.19 cc/m^2-day. Similarly, other temperature comparisons show a consistent pattern of increased OTR with higher temperature.

An increase in MMT concentration from 1% to 2% (at constant vanillin concentration and temperature) generally leads to a decrease in OTR. For instance, comparing samples MT01VA3T50 and MT02VA3T50, the OTR decreases from 283.52 cc/m^2-day to 168.93 cc/m^2-day when MMT concentration increases from 1% to 2%. Similarly, the effect of MMT concentration on OTR is

observable across the samples. When comparing the effect of vanillin concentration on the oxygen transmission rate, the data shows that at a constant MMT concentration and temperature, an increase in vanillin concentration generally results in a decrease in OTR. For example, samples MT01VA3T50 and MT01VA7T50, both at 1% MMT and 50°C, but differing vanillin concentrations (3% and 7%), show a decrease in OTR from 283.52 cc/m^2-day to 226.08 cc/m^2-day. As to the plausible interaction among the variables, there appears to be significant interactions among MMT, vanillin, and temperature. These interactions may lead to non-linear effects on OTR. For example, the combination of 2% MMT, 3% vanillin, and 60°C temperature results in an OTR of 216.81 cc/m^2-day, while the combination of 1% MMT, 7% vanillin, and 50°C temperature results in an OTR of 226.08 cc/m^2-day. The variability in OTR even within samples with the same factor levels (e.g., 1.5% MMT, 5% vanillin, 55°C) suggests that other unmeasured factors or experimental errors may also influence the OTR. Generally, the data demonstrated a complex interplay between the concentrations of MMT, vanillin, and temperature, with the observed response (oxygen transmission rate) being affected by the levels of each factor and their interactions. Analyzing these results further could provide valuable insights into optimizing the materials and conditions for oxygen transmission rates specifically in food packaging applications.

No.Code	Sample	Oxygen Transmission Rate (cc/m^2-day)
1MT01VA3T50	1%MMT/3%Vanillin/Temp-50C	283.5196
2MT02VA3T50	2%MMT/3%Vanillin/Temp-50C	168.9327
3MT01VA7T50	1%MMT/7%Vanillin/Temp-50C	226.0846
4MT02VA7T50	2%MMT/7%Vanillin/Temp-50C	181.6305
5MT01VA3T60	1%MMT/3%Vanillin/Temp-60C	2248.1947
6MT02VA3T60	2%MMT/3%Vanillin/Temp-60C	216.8108
7MT01VA7T60	1%MMT/7%Vanillin/Temp-60C	455.0877
8MT02VA7T60	2%MMT/7%Vanillin/Temp-60C	886.0706
9MT659VA5T55	0.659%MMT/5%Vanillin/Temp-55C	197.6766
10MT234VA5T55	2.34%MMT/5%Vanillin/Temp-55C	254.5903
11MT15VA163T55	1.5%MMT/1.63%Vanillin/Temp-55C	185.245
12MT15VA836T55	1.5%MMT/0.836%Vanillin/Temp-55C	2910.9974
13MT15VA5T465	1.5%MMT/5%Vanillin/Temp-46.5C	346.2802
14MT15VA5T634	1.5%MMT/5%Vanillin/Temp-63.4C	186.7153
15MT15VA5T55	1.5%MMT/5%Vanillin/Temp-55C	173.2773
16MT15VA5T55	1.5%MMT/5%Vanillin/Temp-55C	314.7555
17MT15VA5T55	1.5%MMT/5%Vanillin/Temp-55C	226.0574
18MT15VA5T55	1.5%MMT/5%Vanillin/Temp-55C	327.8484
19MT15VA5T55	1.5%MMT/5%Vanillin/Temp-55C	144.345

Table 4: Oxygen permeation test results of CMC/Vanillin/MMT Nanoclay

By looking at the bar chart of the oxygen permeation (OTR) of the samples in Figure 4, we can immediately notice the huge spikes in the samples MT01VA3T60 and MT15VA836T55. Since the experimental runs were not replicated, it would be difficult to conclude whether these points were due to changes in the level of the variables or a flaw in either the fabrication of the sample or the testing process, or, in some circumstances, an anomaly in the equipment or the measurement system.

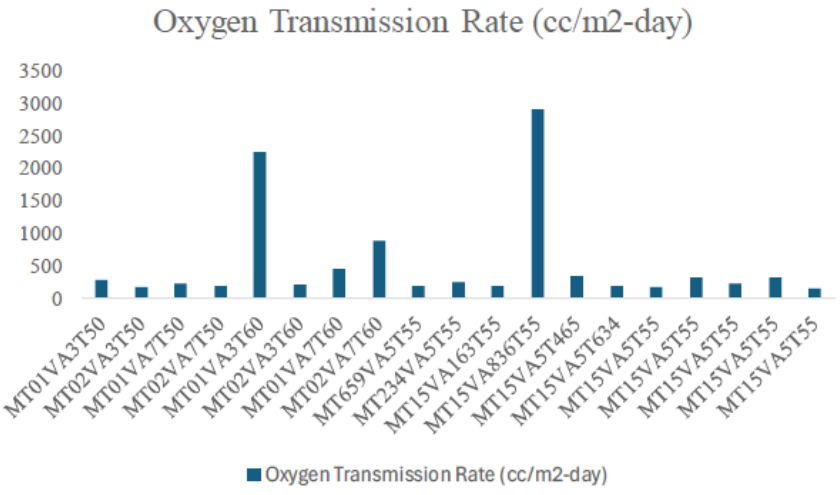

Figure 4: Oxygen permeation of samples

Response Surface Methodology

Table 5 shows the data collected based on a two-level central composite design (CCD) experiment, where the three factors (A, B, and C) are varied at specific levels as defined above. The design includes factorial points, axial points, and center points to capture linear, quadratic, and interaction effects. Factorial points correspond to the combinations of the low and high levels of each factor (-1 and 1). For example, runs 1-8 include the combinations of the lowest and highest levels of A, B, and C. Axial points correspond to the center point of each factor while varying one factor to its extremes (-1.68179 and 1.68179). For example, runs 9 - 14 vary one factor at a time (A, B, or C) while keeping the others at their center points center points. These points (runs 15-19) keep all factors at their center points (0). The repetition of center points helps assess experimental variability and improve the reliability of the results. Notice also that there was a missing datum. In the last run (19), the sample was damaged, leading to the sample unfit for mechanical testing and missing the data for the measured responses.

Std	Run	A	B	C	Code	Sample	Tensile Strength (MPa)	Modulus of Elasticity (Mpa)	Elongation at Break (%)	Oxygen Transmission Rate (cc/m2-day)
1		-1	-1	-1	MT01VA3T50	1%MMT/3%Vanillin/Temp-50C	17.4	537	27	283.5196
2		1	-1	-1	MT02VA3T50	2%MMT/3%Vanillin/Temp-50C	12.7	398	21	168.9327
3		-1	1	-1	MT01VA7T50	1%MMT/7%Vanillin/Temp-50C	14.1	381	28	226.0846
4		1	1	-1	MT02VA7T50	2%MMT/7%Vanillin/Temp-50C	13.1	449	24	181.6305
5		-1	-1	1	MT01VA3T60	1%MMT/3%Vanillin/Temp-60C	11.1	208	44	2248.1947
6		1	-1	1	MT02VA3T60	2%MMT/3%Vanillin/Temp-60C	17.0	742	18	216.8108
7		-1	1	1	MT01VA7T60	1%MMT/7%Vanillin/Temp-60C	16.1	625	23	455.0877
8		1	1	1	MT02VA7T60	2%MMT/7%Vanillin/Temp-60C	15.5	640	17	886.0706
9	-1.68179	0	0	0	MT659VA5T55	0.659%MMT/5%Vanillin/Temp-55C	12.2	370	27	197.6766
10	1.681793	0	0	0	MT234VA5T55	2.34%MMT/5%Vanillin/Temp-55C	16.6	492	34	254.5903
11		0	-1.68179	0	MT15VA163T55	1.5%MMT/1.63%Vanillin/Temp-55C	16.5	684	17	185.2450
12		0	1.681793	0	MT15VA836T55	1.5%MMT/0.836%Vanillin/Temp-55C	14.7	577	27	2910.9974
13		0	0	-1.68179	MT15VA5T465	1.5%MMT/5%Vanillin/Temp-46.5C	11.7	401	21	346.2802
14		0	0	1.681793	MT15VA5T634	1.5%MMT/5%Vanillin/Temp-63.4C	12.7	372	25	186.7153
15		0	0	0	MT15VA5T55	1.5%MMT/5%Vanillin/Temp-55C	11.5	248	39	173.2773
16		0	0	0	MT15VA5T55	1.5%MMT/5%Vanillin/Temp-55C	19.9	628	17	314.7555
17		0	0	0	MT15VA5T55	1.5%MMT/5%Vanillin/Temp-55C	14.7	443	31	226.0574
18		0	0	0	MT15VA5T55	1.5%MMT/5%Vanillin/Temp-55C	17.0	591	27	327.8484
19		0	0	0	MT15VA5T55	1.5%MMT/5%Vanillin/Temp-55C	_*	_*	_*	144.3450

* The sample was damaged

Table 5: Yates' order design for oxygen permeation test results of CMC/Vanillin/MMT Nanoclay

This project takes advantage of the robustness of CCD in the planning and execution of the experiment. The use of a CCD allows for the estimation of the factors' linear, quadratic, and interaction effects on the responses. This design provides information on how the factors influence tensile strength, modulus of elasticity, elongation at break, and oxygen transmission rate.

Depending on the adequacy of the model developed, this study may also aim to optimize the material properties (e.g., high tensile strength, low oxygen transmission rate) by adjusting the factors (A, B, and C). Statistical analysis (e.g., regression) was utilized to identify significant factors and their interactions, and experimental control was achievable especially when the repeated center points provided insight into experimental variability. This CCD data provided a systematic approach to understanding how factors A, B, and C affected the responses and allowed for potential optimization of the material properties.

Response Surface Regression: Tensile Strength (MPa) versus A, B, C

The MINITAB output of the regression coefficients and the summary of the model are shown in Table 6. To provide an intelligent analysis of the given response surface regression data and results, this section focuses on interpreting the statistical findings and what they imply about the factors (A, B, C) and their interactions in relation to tensile strength. Starting from the model performance, it can be shown that the R-squared (R-sq) exhibited an unsatisfactory performance. The R-squared value of 38.64% indicates that the model explains approximately 39% of the variance in tensile strength. This is a relatively low explanatory power, suggesting that there may be other variables not included in the model that significantly influenced the tensile strength. This went along with the very low adjusted R-squared (R-sq(adj)). The adjusted R-squared value, which is 0.00%, suggested that the model may not be effective at predicting tensile strength and might have included irrelevant variables. The same can be observed with the predicted R-squared (R-sq(pred)). The predicted R-squared, which is also 0.00%, may imply that the model has poor predictive power and may perform poorly on new, unseen data.

Term	Coef	SE Coef	T-Value	P-Value	VIF
Constant	14.55	1.20	12.15	0.000	
A	-0.612	0.726	-0.84	0.421	1.00
B	-0.126	0.726	-0.17	0.866	1.00
C	-1.197	0.726	-1.65	0.134	1.00
A*A	-0.000	0.726	-0.00	1.000	1.04
B*B	-0.548	0.726	-0.76	0.469	1.04
C*C	0.795	0.726	1.10	0.302	1.04
A*B	0.200	0.948	0.21	0.838	1.00
A*C	0.125	0.948	0.13	0.898	1.00
B*C	0.275	0.948	0.29	0.778	1.00

Model Summary

S	R-sq	R-sq(adj)	R-sq(pred)
2.68194	38.64%	0.00%	0.00%

Table 6: Coded coefficients and model summary of tensile strength with A (MMT Nanoclay), B (Vanillin), and C (Temperature)

Notice also that none of the factors or interactions have a statistically significant impact on tensile strength, with p-values all above 0.05. This suggests that none of the independent variables (A, B, C) or their combinations are significantly influencing the tensile strength. The linear coefficients for A, B, and C (-0.612, -0.126, and -1.197, respectively) suggest that each factor has a negative impact on tensile strength. The square term coefficients (A*A, B*B, C*C) suggested that while A*A and BB have minimal impact, C*C has a slight positive influence on tensile strength. The interaction term coefficients (A*B, A*C, B*C) are all close to zero, implying that the interactions between the factors do not significantly influence tensile strength. Lastly, the Variance Inflation Factor (VIF) values for all factors and interaction terms are around unity, indicating that multicollinearity is not an issue in the model.

Table 7 exhibits one of the important MINITAB outputs pertaining to the RSM analysis of the tensile strength as one of the responses and the three factors, A, B, and C used in the experiment. Notice how the F-value of 1.04 and p-value of 0.427 suggested that the overall model is not significantly different from the null model (one with just the constant term). This supports the notion that the model does not explain a substantial amount of variance in tensile strength, while the lack-of-fit test ($F = 1.62$, $p = 0.330$) suggests that there might be some lack of fit in the model, but it is not statistically significant.

Source	DF	Adj SS	Adj MS	F-Value	P-Value
Model	9	58128	6458.6	1.14	0.427
Linear	3	33683	11227.6	1.97	0.189
A	1	7572	7572.3	1.33	0.278
B	1	2654	2653.6	0.47	0.512
C	1	23457	23456.8	4.12	0.073
Square	3	9225	3075.0	0.54	0.666
A*A	1	3428	3428.1	0.60	0.457
B*B	1	4582	4582.4	0.81	0.393
C*C	1	3902	3902.3	0.69	0.429
2-Way Interaction	3	15220	5073.3	0.89	0.482
A*B	1	621	621.2	0.11	0.749
A*C	1	10928	10927.7	1.92	0.199
B*C	1	3671	3670.9	0.65	0.442
Error	9	51194	5688.2		
Lack-of-Fit	5	51119	10223.7	543.82	0.000
Pure Error	4	75	18.8		
Total	18	109322			

Regression Equation in Uncoded Units

% Elongation = 20.4 - 14.0 A - 8.3 B - 24.6 C + 5.60 A*A + 6.48 B*B + 5.98 C*C - 3.12 A*B + 13.07 A*C + 7.57 B*C

Table 7: Analysis of variance (ANOVA) of tensile strength with A (MMT Nanoclay), B (Vanillin), and C (Temperature)

The model's low R-squared and adjusted R-squared values indicated that the current model may not be effective at explaining the variation in tensile strength. None of the independent variables or their interactions appeared to have a statistically significant effect on tensile strength. Since RSM as applied to a structured experimentation is a sequential process, it would be advisable as a next step to consider exploring other variables or combinations that may have a greater impact on tensile strength. The lack-of-fit test suggested potential for a better model fit if other variables are incorporated or a different model is used. Potential next steps could involve testing additional independent variables or transforming the current variables to identify a more effective model, given the poor performance of the preliminary model.

Response Surface Regression: Modulus of Elasticity (MPa) versus A, B, C

The response surface regression data provided in Table 8 outlines the relationship between the modulus of elasticity (MPa) and independent variables A, B, and C. Analyzing the model and results based on the model performance may have to be started by looking at the R-squared value of 28.45% which suggests that the model explains approximately 28% of the variance in the modulus of elasticity. This indicates a low level of explanatory power. Moreover, the adjusted R-squared (R-sq(adj)) value of 0.00% implies that the model does not provide meaningful

information beyond the mean of the response variable, while the predicted R-squared (R-sq(pred)), which is also 0.00%, indicated that the model is unlikely to perform well on new set of data.

Term	Coef	SE Coef	T-Value	P-Value	VIF
Constant	528.6	78.4	6.74	0.000	
A	-38.8	47.5	-0.82	0.434	1.00
B	-17.8	47.5	-0.37	0.717	1.00
C	-40.5	47.5	-0.85	0.416	1.00
A*A	5.4	47.5	0.11	0.913	1.04
B*B	-48.2	47.5	-1.01	0.337	1.04
C*C	-15.8	47.5	-0.33	0.746	1.04
A*B	-13.1	62.0	-0.21	0.837	1.00
A*C	-8.8	62.0	-0.14	0.891	1.00
B*C	56.4	62.0	0.91	0.387	1.00

Model Summary

S	R-sq	R-sq(adj)	R-sq(pred)
175.479	28.45%	0.00%	0.00%

Table 8: Coded coefficients and model summary of modulus of elasticity with A (MMT Nanoclay), B (Vanillin), and C (Temperature)

All terms, as can be observed in Table 8, including linear terms (A, B, C), square terms (A*A, B*B, C*C), and interactions (A*B, A*C, B*C), have p-values greater than 0.05, indicating none are statistically significant. All the terms also have negative coefficients, suggesting they decrease the modulus of elasticity, but none of these coefficients are statistically significant. It is also noticeable that A*A may have a minimal positive impact, while B*B and C*C have negative effects, but again, none of these effects are statistically significant. The interaction terms, A*B and A*C have small negative coefficients, while B*C has a larger positive coefficient. Again, all interaction terms are statistically insignificant. Meanwhile, all VIF values around 1 suggested that there may have no issue with multicollinearity among the variables.

The F-value of 0.40 and p-value of 0.907 listed in Table 9 may be an indication that the model is not significantly different from a null model, which means the model does not explain much of the variance in the response variable. The lack-of-fit test ($F = 2.32$, $p = 0.218$), on the other hand, suggests the model fits the data relatively well, as the lack-of-fit is not statistically significant.

Source	DF	Adj SS	Adj MS	F-Value	P-Value
Model	9	110197	12244.1	0.40	0.907
Linear	3	47332	15777.3	0.51	0.684
A	1	20610	20610.0	0.67	0.434
B	1	4315	4315.0	0.14	0.717
C	1	22407	22407.1	0.73	0.416
Square	3	35396	11798.6	0.38	0.768
A*A	1	393	392.7	0.01	0.913
B*B	1	31712	31712.4	1.03	0.337
C*C	1	3429	3429.1	0.11	0.746
2-Way Interaction	3	27470	9156.5	0.30	0.827
A*B	1	1373	1372.6	0.04	0.837
A*C	1	617	616.5	0.02	0.891
B*C	1	25480	25480.4	0.83	0.387
Error	9	277135	30792.8		
Lack-of-Fit	5	206009	41201.9	2.32	0.218
Pure Error	4	71126	17781.5		
Total	18	387333			

Regression Equation in Uncoded Units

Modulus of Elasticity (MPa) = 528.6 - 23.1 A - 10.6 B - 24.1 C + 1.9 A*A - 17.0 B*B - 5.6 C*C - 4.6 A*B - 3.1 A*C + 20.0 B*C

Table 9: Analysis of variance (ANOVA) of modulus of elasticity with A (MMT Nanoclay), B (Vanillin), and C (Temperature)

It has been shown that the response surface model for the modulus of elasticity has limited explanatory and predictive power, as evidenced by the low R-squared and adjusted R-squared values, as well as the lack of statistical significance of the coefficients. The linear and interaction terms suggested that A, B, and C individually and in combination do not significantly influence the modulus of elasticity. The quadratic terms also do not provide significant information regarding the response variable. As the succeeding step, it would be helpful to consider exploring additional variables or different modeling approaches that may better capture the variation in the modulus of elasticity.

The lack-of-fit test suggests there might be room for improvement in the model, as there could be other factors not considered in this model that explain the variability in the response. Since none of the factors are statistically significant, focus should be placed on identifying other potential variables or transformations of the current variables to improve model performance.

Response Surface Regression: % Elongation versus A, B, C

Table 10 outlines the response surface regression data that provided the relationship between the percentage of elongation and independent variables A,

B, and C. The model performance provided the R-squared value of 53.17% which indicated that the model explains approximately 53% of the variance in the percentage of elongation. This indicates a moderate level of explanatory power. The adjusted R-squared (R-sq(adj)) value of 6.34% may imply that the model does not fully capture the variability of the data and may include irrelevant variables. The predicted R-squared (R-sq(pred)), which is 0.00%, is a very low value and can be an indication that the model may not perform well on new set of data.

Term	Coef	SE Coef	T-Value	P-Value	VIF
Constant	20.4	33.7	0.60	0.560	
A	-23.5	20.4	-1.15	0.278	1.00
B	-13.9	20.4	-0.68	0.512	1.00
C	-41.4	20.4	-2.03	0.073	1.00
A*A	15.8	20.4	0.78	0.457	1.04
B*B	18.3	20.4	0.90	0.393	1.04
C*C	16.9	20.4	0.83	0.429	1.04
A*B	-8.8	26.7	-0.33	0.749	1.00
A*C	37.0	26.7	1.39	0.199	1.00
B*C	21.4	26.7	0.80	0.442	1.00

Model Summary

S	R-sq	R-sq(adj)	R-sq(pred)
75.4203	53.17%	6.34%	0.00%

Table 10: Coded coefficients and model summary of percent elongation with A (MMT Nanoclay), B (Vanillin), and C (Temperature)

From Table 10, only the coefficient for C has a p-value approaching significance ($p = 0.073$), while the other coefficients for the linear terms (A and B) and the quadratic terms (A*A, B*B, C*C) are not statistically significant. None of the interaction terms (A*B, A*C, B*C) are statistically significant. All factors have negative coefficients, suggesting they decrease the percentage of elongation, but none of these coefficients, except marginally for C, are statistically significant. All have positive coefficients, suggesting they increase the percentage of elongation.

However, none of these coefficients are statistically significant. As to the interaction terms, AB has a small negative effect, while A*C and B*C have larger positive effects. However, none of these interaction terms are statistically significant. All VIF values were around 1 which may suggest that there is no issue with multicollinearity among the variables.

Source	DF	Adj SS	Adj MS	F-Value	P-Value
Model	9	58128	6458.6	1.14	0.427
Linear	3	33683	11227.6	1.97	0.189
A	1	7572	7572.3	1.33	0.278
B	1	2654	2653.6	0.47	0.512
C	1	23457	23456.8	4.12	0.073
Square	3	9225	3075.0	0.54	0.666
A*A	1	3428	3428.1	0.60	0.457
B*B	1	4582	4582.4	0.81	0.393
C*C	1	3902	3902.3	0.69	0.429
2-Way Interaction	3	15220	5073.3	0.89	0.482
A*B	1	621	621.2	0.11	0.749
A*C	1	10928	10927.7	1.92	0.199
B*C	1	3671	3670.9	0.65	0.442
Error	9	51194	5688.2		
Lack-of-Fit	5	51119	10223.7	543.82	0.000
Pure Error	4	75	18.8		
Total	18	109322			

Regression Equation in Uncoded Units

% Elongation = 20.4 - 14.0 A - 8.3 B - 24.6 C + 5.60 A*A + 6.48 B*B + 5.98 C*C - 3.12 A*B + 13.07 A*C + 7.57 B*C

Table 11: Analysis of variance (ANOVA) of percent elongation with A (MMT Nanoclay), B (Vanillin), and C (Temperature)

The Analysis of Variance (ANOVA) for the elongation with the three factors is shown in Table 11. This table breaks down the total variability in the data into two sources: model and error. The F-value (1.14) and its corresponding p-value (0.427) suggest that the model does not explain a statistically significant portion of the variance in the data. This is consistent with the low R-squared values observed in the model summary table. The lack-of-fit test specifically assesses how well the model fits the data. A statistically significant lack-of-fit (p-value of 0.000 in this case) indicates that the model does not adequately capture the relationship between the factors and the percent elongation. The regression equation shows the relationship between the factors and the predicted percent elongation. It can be used to predict the elongation for a given combination of factors A, B, and C. However, considering the limitations highlighted above, the predictions made by this model may not be very reliable. The results of the response surface regression analysis for the elongation as the response suggested that the model does not adequately capture the relationship between factors A, B, C, and the percent elongation. The model explains a moderate portion of the variance in the data statistically significant. There is also evidence of lack-of-fit, indicating that the model may not be suitable for making predictions.

Response Surface Regression: O_2 Permeation (cc/m^2-day) versus A, B, C

Table 12 as shown below contains the response surface regression results numerically describing how the independent variables A, B, and C, as well as their

squares and interactions, relate to oxygen permeation. From the table, the R-squared value of 54.95% suggests that the model explains approximately 55% of the variance in oxygen permeation. This indicates a moderate level of explanatory power. An adjusted R-squared (R-sq(adj)) value of 9.89% implies that the model does not fully capture the variability of the data and may also include irrelevant variables. The predicted R-squared (R-sq(pred)) value of 0.00%, indicates the model is unlikely to satisfactorily perform on another round of data.

Term	Coef	SE Coef	T-Value	P-Value	VIF
Constant	242	319	0.76	0.467	
A	-122	193	-0.63	0.544	1.00
B	250	193	1.30	0.227	1.00
C	196	193	1.02	0.336	1.00
A*A	-30	193	-0.16	0.879	1.04
B*B	437	193	2.26	0.050	1.04
C*C	-16	193	-0.08	0.936	1.04
A*B	317	252	1.25	0.241	1.00
A*C	-180	252	-0.71	0.493	1.00
B*C	-135	252	-0.53	0.606	1.00

Model Summary

S	R-sq	R-sq(adj)	R-sq(pred)
713.457	54.95%	9.89%	0.00%

Table 12: Coded coefficients and model summary of oxygen permeation with A (MMT Nanoclay), B (Vanillin), and C (Temperature)

Analyzing the p-values in Table 11, generally, most of the terms are not statistically significant ($p > 0.05$), including the linear terms A, B, and C, as well as the interactions (A*B, A*C, B*C). The only exception is the quadratic term B*B, which has a p-value of 0.050, suggesting marginal significance. As for the linear terms of the model, A has a negative effect (-122), while B and C both have positive effects (250 and 196, respectively). The oxygen permeation model's quadratic terms A*A and C*C have minimal impact on oxygen permeation, while B*B has a significant positive impact (437). Interaction terms A*B, A*C, and B*C have some impact on oxygen permeation but are not statistically significant, suggesting that interactions among the factors may not be strong influencers. Variance Inflation Factor (VIF) values were consistently around 1 suggesting that there is no issue with multicollinearity among the variables.

Source	DF	Adj SS	Adj MS	F-Value	P-Value
Model	9	5586813	620757	1.22	0.386
Linear	3	1581904	527301	1.04	0.422
A	1	202681	202681	0.40	0.544
B	1	854230	854230	1.68	0.227
C	1	524994	524994	1.03	0.336
Square	3	2797965	932655	1.83	0.212
A*A	1	12562	12562	0.02	0.879
B*B	1	2607445	2607445	5.12	0.050
C*C	1	3523	3523	0.01	0.936
2-Way Interaction	3	1206944	402315	0.79	0.529
A*B	1	801694	801694	1.57	0.241
A*C	1	259690	259690	0.51	0.493
B*C	1	145560	145560	0.29	0.606
Error	9	4581190	509021		
Lack-of-Fit	5	4554126	910825	134.62	0.000
Pure Error	4	27064	6766		
Total	18	10168004			

Regression Equation in Uncoded Units

O2 Permeation (cc/m2-day) = 242 - 72 A + 149 B + 117 C - 10.7 A*A + 154.5 B*B - 5.7 C*C + 111.9 A*B - 63.7 A*C - 47.7 B*C

Table 13: Analysis of variance (ANOVA) of oxygen permeation with A (MMT Nanoclay), B (Vanillin), and C (Temperature)

From the ANOVA table of oxygen permeation in Table 13, it can be observed that the F-value of 1.22 and p-value of 0.386 indicate that the model is not significantly different from a null model. Therefore, the model may not adequately explain the variation in oxygen permeation. The lack-of-fit test shows an extremely high F-value (134.62) and a significant p-value (0.000), indicating that the model does not fit the data well and there may be other important variables or interactions not captured in the model. The current model has moderate explanatory power (R-squared of 54.95%) but limited predictive power (predicted R-squared of 0.00%).

Most of the coefficients, except for B*B, are not statistically significant, suggesting that many of the factors may not have a meaningful impact on oxygen permeation. The significant lack-of-fit indicates a need for model refinement, either by adding more relevant variables or considering a different modeling approach. Given the results, consider focusing on B*B for its marginal significance and potential impact on oxygen permeation. The interactions among the variables (A*B, A*C, B*C) do not seem to be strong influencers; thus, these terms may not need to be included in future models. Since the oxygen permeation response showed a significant factor in the identity of the vanillin concentration, it is believed to be worthy of looking more closely. Figure 5 shown below is the half normal probability plot of the standardized effects highlighting B*B as the term in the model that has a significant effect on the oxygen permeation, while the normal probability plot in Figure 6 shows the residuals almost clustered and assembled along the diagonal line. This trend may be an indication that the data

closely resemble normality behavior.

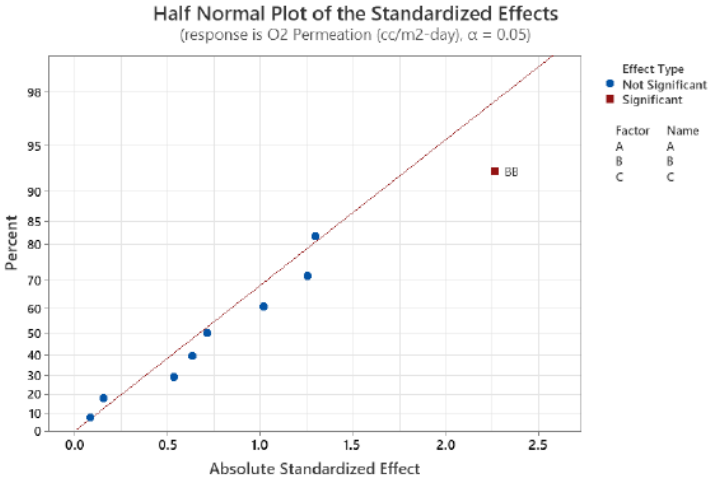

Figure 5: Half-normal plot of the standardized effects of the oxygen permeation rate

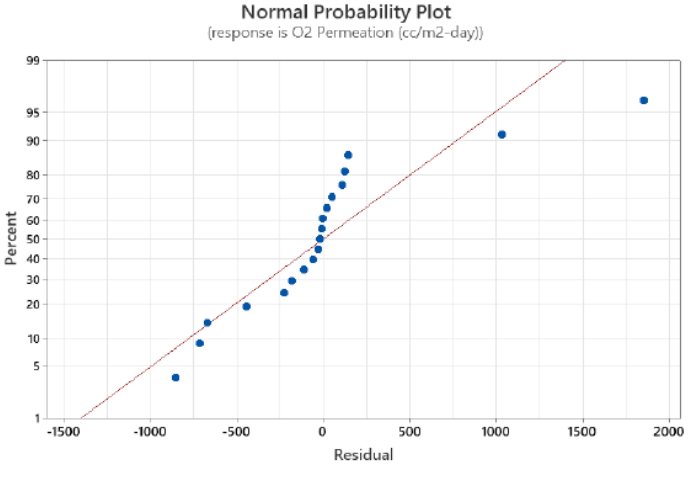

Figure 6: Normal probability plot of the residual of the oxygen permeation rate

Figure 7 shows the surface plot of oxygen permeation with nanoclay and vanillin concentration. As shown in this plot, there are two noticeable negative spikes at high level of vanillin – low level MMT, and low level of vanillin – moderate level MMT. These areas became more pronounced when displayed through contour plots shown in Figures 8 and 9, and these regions could potentially be the area at which the minimum points are situated.

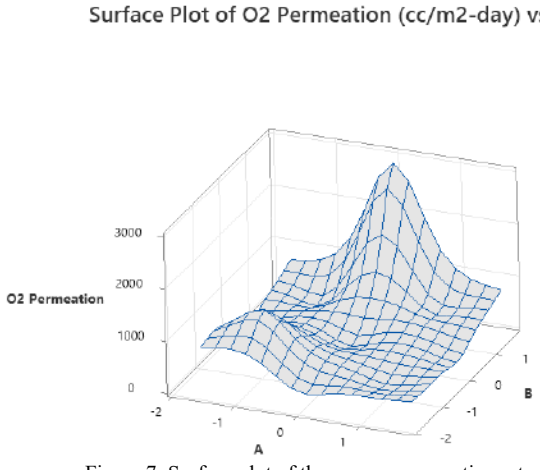

Figure 7: Surface plot of the oxygen permeation rate

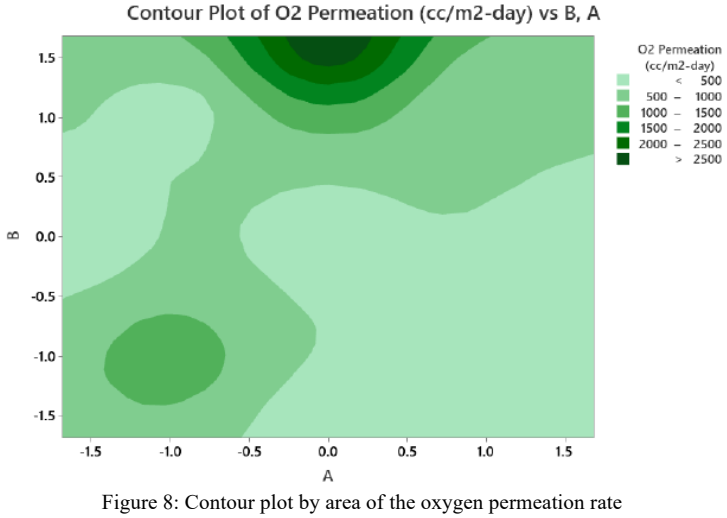

Figure 8: Contour plot by area of the oxygen permeation rate

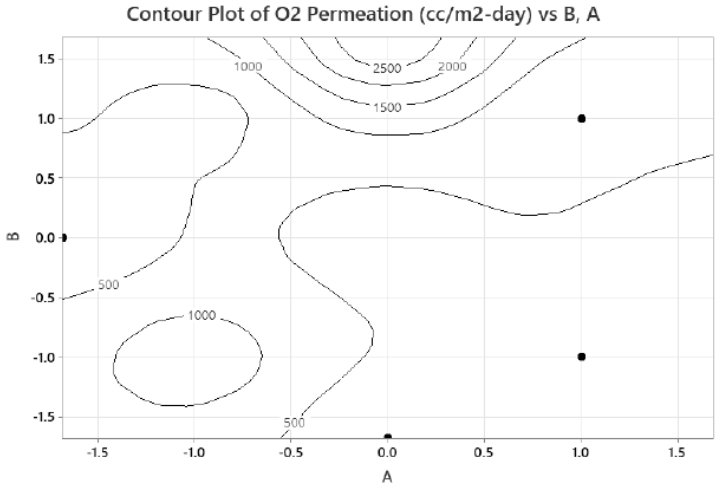

Figure 9: Contour plot by lines of the oxygen permeation rate

The results of the response surface regression analysis for each of the response suggested that the models do not adequately capture the relationship between factors A, B, C, and the responses. There were models that could explain a moderate portion of the variance in the data statistically significant, but the evidence of the presence of lack-of-fit indicated that the model may not be suitable for making predictions.

Transmission Electron Microscopy

Figure 10 shows the TEM images of the intercalated clay particles into polylactic acid (PLA) matrix [161] while Figure 11 is a collection of TEM images in this project showing MMT nanoclay intercalated into CMC-vanillin blend. As can be seen in Figure 11, the nanoclay was about 20 nm in diameter but it was sparsely distributed into the bed of CMC and vanillin film. This thinly scattered MMT nanoparticles does not seem to have formed a fully developed tortuous path and this might have been attributed to insufficient amount of the added nanoclay.

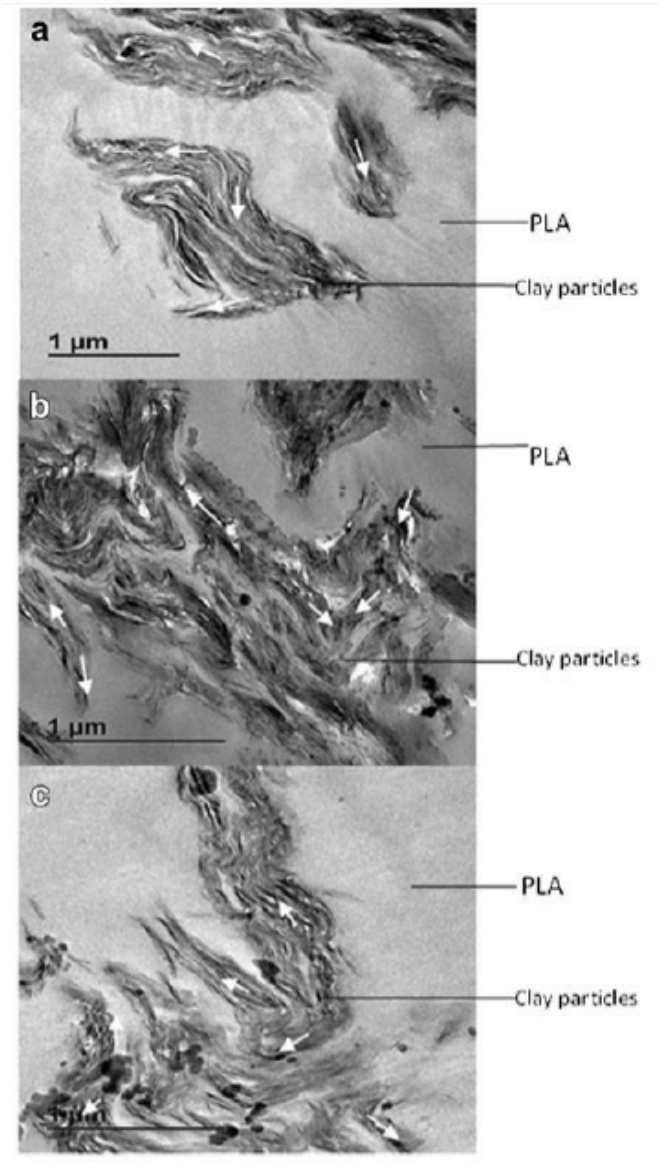

Figure 10: TEM images showing the intercalated PLA into the clay galleries from the paper of Cele et. al. (2014).

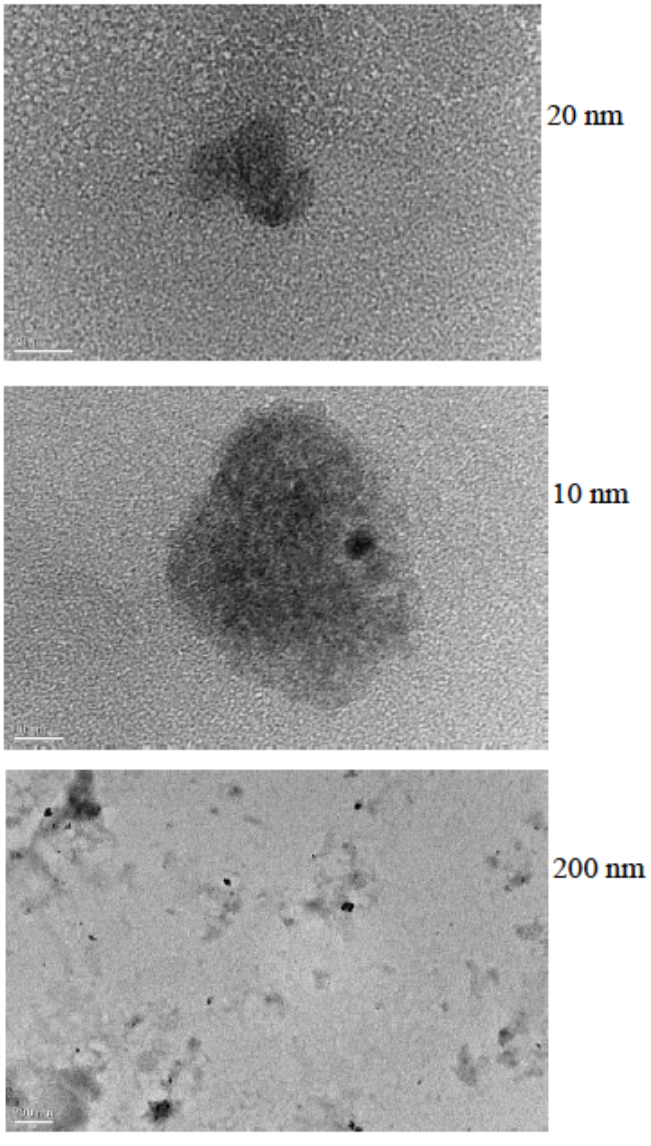

Figure 11: TEM images showing the intercalated MMT nanoclay 20 nm diameter.

The MMT nanoclay in the project as shown in the TEM image in Figure 12 was believed to be fully intercalated since there is close resemblance with the TEM image shown in Figure 13 of intercalated MMT in other published paper [162].

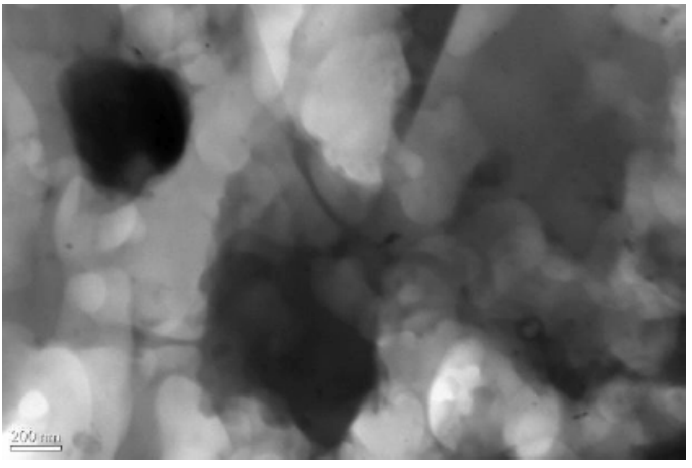

Figure 12: TEM image of MMT nanoclay intercalated into CMC.

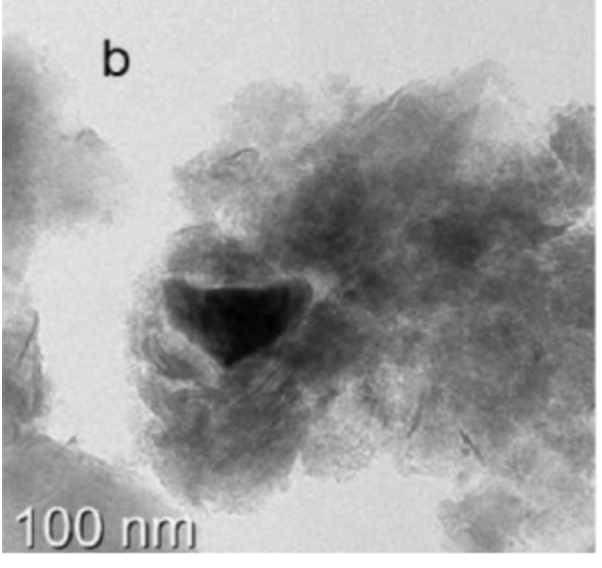

Figure 13: TEM image of montmorillonite clay after treatment with PDSA from the paper of Venkatesha et. al. (2015).

Conclusion

There has been a growing interest to shift from the use of petroleum-derived materials to sustainable, environment-friendly alternatives. This as part of the recent quest for ways to at least alleviate, if cannot be totally mitigated, the challenges that the world is confronting with the environment. This project

successfully fabricated a prototype of a packaging film from biomaterials (i.e., carboxymethyl cellulose, vanillin, and nanoclay). This nanocomposite film was formulated in different compositions according to a rotatable central composite design (response surface methodology) in an attempt to determine the optimum formulation. However, the current models for all four responses (tensile strength, modulus of elasticity, elongation, and oxygen permeation) which demonstrated limited effectiveness in explaining the variation in the respective outcomes. This is evident from the low R-squared and adjusted R-squared values, lack of statistical significance in most coefficients and interactions, and significant lack-of-fit tests across the board. Given the poor predictive power of the models and lack of significant impact of the independent variables, the current approaches and modeling techniques require re-evaluation. To be able to improve the explanatory and predictive capabilities of the models, further analysis and refinement may be necessary. Future efforts should focus on exploring additional variables like sample conditioning. It was observed that there was a significant increase in tensile strength upon storage (48h or more at ambient conditions). The use of transformation on the responses with the current variables and evaluating different transformations of these variables to enhance model fit and explanatory power might also be part of future work and adapting different modeling approaches or considering alternative modeling techniques or functional forms to better capture the relationships between the variables and the responses. The range of the level of each factor should also be stretched far enough for the responses to deliver significant magnitude or to be able for the responses to bring discriminate measurements. It may also be helpful to perform a measurement system analysis (MSA) or a gauge repeatability and reproducibility (GR&R) on the machines that are being used for measurement of the responses to determine or validate their measurement capability or their capacity to deliver their intended purpose. RSM is a sequential or iterative process [163], [164], [165] and because of the sequential nature of its approach, the results of the project may be part of an important preliminary trials whose data and learning experiences necessary for successful implementation of the succeeding experiments. Most of the OTR values, between 150 and 1000 cc/m^2day, can be considered breathable films. Case ready meat, fish, sausage, fresh produce and vegetables, and other food goods needing breathable films can be wrapped with these blended compositions, which offer films and/or film structures with a mix of oxygen breathability, high formability, and structural strength.

Bibliography

1. S. Mehariya, M. Plöhn, P. Jablonski, S. Stagge, L. J. Jönsson, and C. Funk, “Biopolymer production from biomass produced by Nordic microalgae grown in wastewater,” Bioresour. Technol., vol. 376, no. January, 2023, doi: 10.1016/j.biortech.2023.128901.
2. A. Jayakumar et al., “Recent innovations in bionanocomposites-based food packaging films – A comprehensive review,” Food Packag. Shelf Life, vol. 33,

no. May, p. 100877, 2022, doi: 10.1016/j.fpsl.2022.100877.
3. R. Geyer, “Production, use, and fate of synthetic polymers,” in Plastic Waste and Recycling: Environmental Impact, Societal Issues, Prevention, and Solutions, T. M. Letcher, Ed., Academic Press, 2020, pp. 13–32. [Online]. Available: https://doi.org/10.1016/C2018-0-01939-8
4. A. Chamas et al., “Degradation Rates of Plastics in the Environment,” ACS Sustain. Chem. Eng., vol. 8, no. 9, pp. 3494–3511, 2020, doi: 10.1021/acssuschemeng.9b06635.
5. Hannah Ritchie, “How much plastic waste ends up in the ocean?,” 2023. https://ourworldindata.org/how-much-plastic-waste-ends-up-in-the-ocean (accessed Mar. 19, 2024).
6. Y. Su et al., “Steam disinfection releases micro(nano)plastics from silicone-rubber baby teats as examined by optical photothermal infrared microspectroscopy,” Nat. Nanotechnol., vol. 17, no. 1, pp. 76–85, 2022, doi: 10.1038/s41565-021-00998-x.
7. J. Zhang et al., “Identification of Poly(ethylene terephthalate) Nanoplastics in Commercially Bottled Drinking Water Using Surface-Enhanced Raman Spectroscopy,” Environ. Sci. Technol., vol. 57, no. 22, pp. 8365–8372, 2023, doi: 10.1021/acs.est.3c00842.
8. G. Shin, D. Lim, and D. Shin, “Plasmonic heating effect in SERS-based nanoplastic detection,” Sensors Actuators B Chem., vol. 393, no. June, p. 134196, 2023, doi: 10.1016/j.snb.2023.134196.
9. Y. K. Song et al., “A comparison of microscopic and spectroscopic identification methods for analysis of microplastics in environmental samples,” Mar. Pollut. Bull., vol. 93, no. 1–2, pp. 202–209, 2015, doi: 10.1016/j.marpolbul.2015.01.015.
10. A. McCormick, T. J. Hoellein, S. A. Mason, J. Schluep, and J. J. Kelly, “Microplastic is an abundant and distinct microbial habitat in an urban river,” Environ. Sci. Technol., vol. 48, no. 20, pp. 11863–11871, 2014, doi: 10.1021/es503610r.
11. K. Jabeen et al., “Microplastics and mesoplastics in fish from coastal and fresh waters of China,” Environ. Pollut., vol. 221, pp. 141–149, 2017, doi: 10.1016/j.envpol.2016.11.055.
12. X. X. Zhou, R. Liu, L. T. Hao, and J. F. Liu, “Identification of polystyrene nanoplastics using surface enhanced Raman spectroscopy,” Talanta, vol. 221, no. August 2020, p. 121552, 2021, doi: 10.1016/j.talanta.2020.121552.
13. C. J. Rhodes, “Plastic pollution and potential solutions,” Sci. Prog., vol. 101, no. 3, pp. 207–260, 2018, doi: 10.3184/003685018X15294876706211.
14. Y. Khairnar et al., “Cellulose bionanocomposites for sustainable planet and people: A global snapshot of preparation, properties, and applications,” Carbohydr. Polym. Technol. Appl., vol. 2, no. March, p. 100065, 2021, doi: 10.1016/j.carpta.2021.100065.
15. A. K. Antosik, K. Mozelewska, M. Musik, P. Miądlicki, J. Sreńscek-Nazzal, and K. Wilpiszewska, “The effect of neat and modified montmorillonite on thermal properties of silicone pressure-sensitive adhesives,” Int. J. Adhes. Adhes., vol. 130, 2024, doi: 10.1016/j.ijadhadh.2023.103609.

16. Anilkumar, S. Anisree, K. V. Pradeep Kumar, R. Kanojia, A. Shanmugam, and M. Parthasarathy, “Preparation and characterization of polyvinyl alcohol nanofibers/polyanyline-montmorillonite clay,” Mater. Today Proc., no. May, 2023, doi: 10.1016/j.matpr.2023.08.314.
17. S. Vaud et al., “Jo ur r f,” Metab. Eng., p. 100883, 2021, doi: 10.1016/j.ceramint.2024.03.194.
18. S. Zhou et al., “Low-cost and high-safety montmorillonite-based solid electrolyte for lithium metal batteries,” Appl. Clay Sci., vol. 251, no. January, p. 107329, 2024, doi: 10.1016/j.clay.2024.107329.
19. R. Sun et al., “Preparation and characterization of pectin-alginate-based microbeads reinforced by nano montmorillonite filler for probiotics encapsulation: Improving viability and colonic colonization,” Int. J. Biol. Macromol., vol. 264, no. P1, p. 130543, 2024, doi: 10.1016/j.ijbiomac.2024.130543.
20. Y. Ke et al., “Feather keratin-montmorillonite nanocomposite hydrogel promotes bone regeneration by stimulating the osteogenic differentiation of endogenous stem cells,” Int. J. Biol. Macromol., vol. 243, no. April, 2023, doi: 10.1016/j.ijbiomac.2023.125330.
21. P. R. Chinnam, H. Zhang, and S. L. Wunder, “Blends of pegylated polyoctahedralsilsesquioxanes (POSS-PEG) and methyl cellulose as solid polymer electrolytes for lithium batteries,” Electrochim. Acta, vol. 170, pp. 191–201, 2015, doi: 10.1016/j.electacta.2015.04.010.
22. N. P. Risyon, S. H. Othman, R. K. Basha, and R. A. Talib, “Characterization of polylactic acid/halloysite nanotubes bionanocomposite films for food packaging,” Food Packag. Shelf Life, vol. 23, no. May 2019, p. 100450, 2020, doi: 10.1016/j.fpsl.2019.100450.
23. J. R. A. Pires, V. G. L. de Souza, and A. L. Fernando, “Chitosan/montmorillonite bionanocomposites incorporated with rosemary and ginger essential oil as packaging for fresh poultry meat,” Food Packag. Shelf Life, vol. 17, no. June, pp. 142–149, 2018, doi: 10.1016/j.fpsl.2018.06.011.
24. S. DRITSAS, Y. VIJAY, S. HALIM, R. TEO, N. SANANDIYA, and J. G. FERNANDEZ, “Cellulosic Biocomposites for Sustainable Manufacturing,” Fabr. 2020, pp. 74–81, 2020, doi: 10.2307/j.ctv13xpsvw.14.
25. R. L. C. G. da Silva, O. D. Bernardinelli, E. C. G. Frachini, H. Ulrich, E. Sabadini, and D. F. S. Petri, “Vanillin crosslinked chitosan films: The states of water and the effect of carriers on curcumin uptake,” Carbohydr. Polym., vol. 292, no. March, p. 119725, 2022, doi: 10.1016/j.carbpol.2022.119725.
26. S. Beigzadeh Ghelejlu, M. Esmaiili, and H. Almasi, “Characterization of chitosan-nanoclay bionanocomposite active films containing milk thistle extract,” Int. J. Biol. Macromol., vol. 86, pp. 613–621, 2016, doi: 10.1016/j.ijbiomac.2016.02.012.
27. M. Kaur, M. Arshad, and A. Ullah, “In-Situ Nanoreinforced Green Bionanomaterials from Natural Keratin and Montmorillonite (MMT)/Cellulose Nanocrystals (CNC),” ACS Sustain. Chem. Eng., vol. 6, no. 2, pp. 1977–1987, 2018, doi: 10.1021/acssuschemeng.7b03380.

28. Q. Ke, H. Wang, X. Huang, Y. Zhang, Q. Meng, and X. Kou, “Direct addition of vanillin improved the physicochemical properties and antibacterial activities of gelatin/sodium carboxymethyl cellulose composite film,” Ind. Crops Prod., vol. 206, no. August, p. 117653, 2023, doi: 10.1016/j.indcrop.2023.117653.
29. C. M. O. Müller, J. B. Laurindo, and F. Yamashita, “Effect of nanoclay incorporation method on mechanical and water vapor barrier properties of starch-based films,” Ind. Crops Prod., vol. 33, no. 3, pp. 605–610, 2011, doi: 10.1016/j.indcrop.2010.12.021.
30. H. Mohammadi, A. Kamkar, and A. Misaghi, “Nanocomposite films based on CMC, okra mucilage and ZnO nanoparticles: Physico mechanical and antibacterial properties,” Carbohydr. Polym., vol. 181, no. August 2017, pp. 351–357, 2018, doi: 10.1016/j.carbpol.2017.10.045.
31. H. Nabeel Ahmad, Y. Yong, S. Wang, N. Munawar, and J. Zhu, “Development of novel carboxymethyl cellulose/gelatin-based edible films with pomegranate peel extract as antibacterial/antioxidant agents for beef preservation,” Food Chem., vol. 443, no. October 2023, p. 138511, 2024, doi: 10.1016/j.foodchem.2024.138511.
32. R. Eshaghi, M. Mohsenzadeh, and J. F. Ayala-Zavala, “Bio-nanocomposite active packaging films based on carboxymethyl cellulose, myrrh gum, TiO2 nanoparticles and dill essential oil for preserving fresh-fish (Cyprinus carpio) meat quality,” Int. J. Biol. Macromol., no. February 2023, p. 129991, 2024, doi: 10.1016/j.ijbiomac.2024.129991.
33. A. Singh, J. Singh, N. Singh, and N. Kaur, “Development and characterization of gelatin/carboxymethyl cellulose based polymeric film with inclusion of ionic liquid to enhance the shelf life of food,” Food Packag. Shelf Life, vol. 42, no. August 2023, p. 101251, 2024, doi: 10.1016/j.fpsl.2024.101251.
34. L. Abolghasemi Fakhri, B. Ghanbarzadeh, J. Dehghannya, F. Abbasi, and H. Ranjbar, “Optimization of mechanical and color properties of polystyrene/nanoclay/nano ZnO based nanocomposite packaging sheet using response surface methodology,” Food Packag. Shelf Life, vol. 17, no. April, pp. 11–24, 2018, doi: 10.1016/j.fpsl.2018.04.005.
35. C. S. Araújo, A. M. C. Rodrigues, M. R. S. Peixoto Joele, E. A. F. Araújo, and L. F. H. Lourenço, “Optmizing process parameters to obtain a bioplastic using proteins from fish byproducts through the response surface methodology,” Food Packag. Shelf Life, vol. 16, no. January, pp. 23–30, 2018, doi: 10.1016/j.fpsl.2018.01.009.
36. M. R. V. Bertolo et al., “Central composite design optimization of active and physical properties of food packaging films based on chitosan/gelatin/pomegranate peel extract,” Food Packag. Shelf Life, vol. 34, no. November, 2022, doi: 10.1016/j.fpsl.2022.100986.
37. B. Tomadoni, A. Ponce, M. Pereda, and M. R. Ansorena, “Vanillin as a natural cross-linking agent in chitosan-based films: Optimizing formulation by response surface methodology,” Polym. Test., vol. 78, no. June, p. 105935, 2019, doi: 10.1016/j.polymertesting.2019.105935.
38. H. Yin et al., “Optimization of antibacterial and physical properties of

chitosan/citronella oil film by electrostatic spraying and evaluation of its preservation effectiveness on salmon fillets," Food Packag. Shelf Life, vol. 33, no. January, 2022, doi: 10.1016/j.fpsl.2022.100891.
39. M. Yılmaz and A. Altan, "Optimization of functionalized electrospun fibers for the development of colorimetric oxygen indicator as an intelligent food packaging system," Food Packag. Shelf Life, vol. 28, no. September 2020, p. 100651, 2021, doi: 10.1016/j.fpsl.2021.100651.
40. R. Zafar, K. M. Zia, S. Tabasum, F. Jabeen, A. Noreen, and M. Zuber, "Polysaccharide based bionanocomposites, properties and applications: A review," Int. J. Biol. Macromol., vol. 92, pp. 1012–1024, 2016, doi: 10.1016/j.ijbiomac.2016.07.102.
41. Y. Shchipunov, "Bionanocomposites: Green sustainable materials for the near future," Pure Appl. Chem., vol. 84, no. 12, pp. 2579–2607, 2012, doi: 10.1351/PAC-CON-12-05-04.
42. A. K. Khan et al., "Carrageenan based bionanocomposites as drug delivery tool with special emphasis on the influence of ferromagnetic nanoparticles," Oxid. Med. Cell. Longev., vol. 2017, 2017, doi: 10.1155/2017/8158315.
43. A. Ali, S. Bairagi, S. A. Ganie, and S. Ahmed, "Polysaccharides and proteins based bionanocomposites as smart packaging materials: From fabrication to food packaging applications a review," Int. J. Biol. Macromol., vol. 252, no. April, p. 126534, 2023, doi: 10.1016/j.ijbiomac.2023.126534.
44. A. Arora and G. W. Padua, "Review: Nanocomposites in food packaging," J. Food Sci., vol. 75, no. 1, pp. 43–49, 2010, doi: 10.1111/j.1750-3841.2009.01456.x.
45. V. G. L. Souza et al., "Strategies to Improve the Barrier and Mechanical Properties of Pectin Films for Food Packaging: Comparing Nanocomposites with Bilayers," Coatings, vol. 12, no. 2, 2022, doi: 10.3390/coatings12020108.
46. V. G. Bhat, S. P. Masti, S. S. Narasagoudr, R. B. Chougale, P. Kumar, and A. B. Vantamuri, "Development and characterization of Chitosan/Guar gum /Gum ghatti bionanocomposites with in situ silver nanoparticles," Chem. Data Collect., vol. 44, no. February, p. 101009, 2023, doi: 10.1016/j.cdc.2023.101009.
47. E. Marugan, E. P. Rebitski, M. Darder, S. R. G. Balestra, G. del Real, and P. Aranda, "Allantoin-zinc layered simple hydroxide biohybrid as antimicrobial active phase in cellulosic bionanocomposites as potential wound dressings," Applied Clay Science, vol. 241. 2023. doi: 10.1016/j.clay.2023.107002.
48. M. Ali, S. Mir, O. U. R. Abid, A. W. Ajlouni, S. Ghafoor Alvi, and S. Bibi, "Applications Of Chitosan Based Bionanocomposites In Drug-Delivery And Anticancer Treatment-A Review," Eur. Polym. J., vol. 201, no. November, p. 112576, 2023, doi: 10.1016/j.eurpolymj.2023.112576.
49. S. Yoosefi et al., "Dual drug delivery system based on layered double hydroxides/carboxymethyl cellulose-poly ethylene oxide bionanocomposite electrospun fibrous mats: Fabrication, characterization, in-vitro and in-vivo studies," Int. J. Biol. Macromol., vol. 222, no. PB, pp. 3142–3154, 2022, doi: 10.1016/j.ijbiomac.2022.10.087.
50. N. C. P, K. B. S, and S. K. V, "Multifunctional organic and inorganic hybrid

bionanocomposite of chitosan/poly(vinyl alcohol)/nanobioactive glass/nanocellulose for bone tissue engineering," J. Mech. Behav. Biomed. Mater., vol. 135, no. August, p. 105427, 2022, doi: 10.1016/j.jmbbm.2022.105427.
51. M. Rameez, N. Khan, S. Ahmad, and M. M. Ahmad, "Jo ur na l P r f," Biocatal. Agric. Biotechnol., p. 103115, 2024, doi: 10.1016/j.bcab.2024.103115.
52. E. Ravelo-Nieto, S. A. Ovalle-Serrano, E. A. Gutiérrez-Pineda, C. Blanco-Tirado, and M. Y. Combariza, "Textile wastewater depuration using a green cellulose based Fe3O4 bionanocomposite," J. Environ. Chem. Eng., vol. 11, no. 2, 2023, doi: 10.1016/j.jece.2023.109516.
53. M. M. Rahman, "Waste biomass derived chitosan-natural clay based bionanocomposites fabrication and their potential application on wastewater purification by continuous adsorption: A critical review," South African J. Chem. Eng., vol. 48, no. November 2023, pp. 214–236, 2024, doi: 10.1016/j.sajce.2024.02.006.
54. A. K. Das, M. N. Islam, R. K. Ghosh, and R. Maryana, "Cellulose-based bionanocomposites in energy storage applications-A review," Heliyon, vol. 9, no. 1, p. e13028, 2023, doi: 10.1016/j.heliyon.2023.e13028.
55. M. Pourmadadi et al., "Novel carboxymethyl cellulose based nanocomposite: A promising biomaterial for biomedical applications," Process Biochem., vol. 130, no. April, pp. 211–226, 2023, doi: 10.1016/j.procbio.2023.03.033.
56. S. Panahirad et al., "Applications of carboxymethyl cellulose- and pectin-based active edible coatings in preservation of fruits and vegetables: A review," Trends Food Sci. Technol., vol. 110, no. August 2020, pp. 663–673, 2021, doi: 10.1016/j.tifs.2021.02.025.
57. M. S. Rahman et al., "Recent developments of carboxymethyl cellulose," Polymers (Basel)., vol. 13, no. 8, 2021, doi: 10.3390/polym13081345.
58. A. Abdulhameed, H. M. Mbuvi, E. O. Changamu, and F. M. Maingi, "Microwave synthesis of Carboxymethylcellulose (CMC) from Rice Husk," IOSR J. Appl. Chem. (IOSR-JAC, vol. 12, no. December, pp. 33–42, 2019, doi: 10.9790/5736-1212013342.
59. W. Klunklin et al., "Synthesis, Characterization, and Application of Carboxymethyl Cellulose from Asparagus Stalk End," Polymers (Basel)., vol. 13, no. 81, pp. 1–15, 2021.
60. A. K. Singh, R.K., Singh, "Optimization of Reaction Conditions for Preparing Carboxymethyl Cellulose from Corn Cobic Agricultural Waste," Waste and Biomass Valorization, vol. 4, no. 2013, pp. 129–137, 2012, [Online]. Available: https://doi.org/10.1007/s12649-012-9123-9
61. T. Shui et al., "Synthesis of sodium carboxymethyl cellulose using bleached crude cellulose fractionated from cornstalk," Biomass and Bioenergy, vol. 105, pp. 51–58, 2017, doi: 10.1016/j.biombioe.2017.06.016.
62. M. I. H. Mondal, M. S. Yeasmin, and M. S. Rahman, "Preparation of food grade carboxymethyl cellulose from corn husk agrowaste," Int. J. Biol. Macromol., vol. 79, pp. 144–150, 2015, doi: 10.1016/j.ijbiomac.2015.04.061.
63. V. Pushpamalar, S. J. Langford, M. Ahmad, and Y. Y. Lim, "Optimization of

reaction conditions for preparing carboxymethyl cellulose from sago waste," Carbohydr. Polym., vol. 64, no. 2, pp. 312–318, 2006, doi: 10.1016/j.carbpol.2005.12.003.
64. A. H. Abdullah, M. A. A. Awad-Allah, N. A. A. Abd-Elkarim, Z. F. R. Ahmed, and E. M. A. Taha, "Carboxymethyl Cellulose from Banana Rachis: A Potential Edible Coating to Extend the Shelf Life of Strawberry Fruit," Agric., vol. 13, no. 5, 2023, doi: 10.3390/agriculture13051058.
65. M. P. Adinugraha, D. W. Marseno, and Haryadi, "Synthesis and characterization of sodium carboxymethylcellulose from cavendish banana pseudo stem (Musa cavendishii LAMBERT)," Carbohydr. Polym., vol. 62, no. 2, pp. 164–169, 2005, doi: 10.1016/j.carbpol.2005.07.019.
66. F. Yaşar, H. Toğrul, and N. Arslan, "Flow properties of cellulose and carboxymethyl cellulose from orange peel," J. Food Eng., vol. 81, no. 1, pp. 187–199, 2007, doi: 10.1016/j.jfoodeng.2006.10.022.
67. H. Dai and H. Huang, "Enhanced swelling and responsive properties of pineapple peel arboxymethyl cellulose-g-poly(acrylic acid-co-acrylamide) superabsorbent hydrogel by the introduction of carclazyte," J. Agric. Food Chem., vol. 65, no. 3, pp. 565–574, 2017, doi: 10.1021/acs.jafc.6b04899.
68. L. Golbaghi, M. Khamforoush, and T. Hatami, "Carboxymethyl cellulose production from sugarcane bagasse with steam explosion pulping: Experimental, modeling, and optimization," Carbohydr. Polym., vol. 174, pp. 780–788, 2017, doi: 10.1016/j.carbpol.2017.06.123.
69. P. Rachtanapun, S. Luangkamin, K. Tanprasert, and R. Suriyatem, "Carboxymethyl cellulose film from durian rind," Lwt, vol. 48, no. 1, pp. 52–58, 2012, doi: 10.1016/j.lwt.2012.02.029.
70. J. N. Xiaojia He, Shaozu Wu, Dongkang Fu, "Preparation of sodium carboxymethyl cellulose from paper sludge," J. Chem. Technol. Biotechnol., vol. 84, no. 3, pp. 427–434, 2009, [Online]. Available: https://doi.org/10.1002/jctb.2057
71. G. Joshi, S. Naithani, V. K. Varshney, S. S. Bisht, V. Rana, and P. K. Gupta, "Synthesis and characterization of carboxymethyl cellulose from office waste paper: A greener approach towards waste management," Waste Manag., vol. 38, no. 1, pp. 33–40, 2015, doi: 10.1016/j.wasman.2014.11.015.
72. M. I. H. M. A. B. M. Fakrul Alam, "Utilization of cellulosic wastes in textile and garment industries. I. Synthesis and grafting characterization of carboxymethyl cellulose from knitted rag," J. Appl. Polym. Sci., vol. 128, no. 2, pp. 1206–1212, 2013, [Online]. Available: https://doi.org/10.1002/app.38446
73. H. Bidgoli, A. Zamani, A. Jeihanipour, and M. J. Taherzadeh, "Preparation of carboxymethyl cellulose superabsorbents from waste textiles," Fibers Polym., vol. 15, no. 3, pp. 431–436, 2014, doi: 10.1007/s12221-014-0431-5.
74. N. Haleem, M. Arshad, M. Shahid, and M. A. Tahir, "Synthesis of carboxymethyl cellulose from waste of cotton ginning industry," Carbohydr. Polym., vol. 113, pp. 249–255, 2014, doi: 10.1016/j.carbpol.2014.07.023.
75. I. A. Jahan, F. Sultana, M. N. Islam, M. A. Hossain, and J. Abedin, "Studies on Indigenous Cotton linters for Preparation of Carboxymethyl Cellulose,"

Bangladesh J. Sci. Ind. Res., vol. 42, no. 1, pp. 29–36, 1970, doi: 10.3329/bjsir.v42i1.352.
76. J. F. Su, Z. Huang, X. Y. Yuan, X. Y. Wang, and M. Li, "Structure and properties of carboxymethyl cellulose/soy protein isolate blend edible films crosslinked by Maillard reactions," Carbohydr. Polym., vol. 79, no. 1, pp. 145–153, 2010, doi: 10.1016/j.carbpol.2009.07.035.
77. V. Rosilio, G. Albrecht, A. Baszkin, and L. Merle, "Surface properties of hydrophobically modified carboxymethylcellulose derivatives. Effect of salt and proteins," Colloids Surfaces B Biointerfaces, vol. 19, no. 2, pp. 163–172, 2000, doi: 10.1016/S0927-7765(00)00151-X.
78. A. Gregorova, N. Saha, T. Kitano, and P. Saha, "Hydrothermal effect and mechanical stress properties of carboxymethylcellulose based hydrogel food packaging," Carbohydr. Polym., vol. 117, pp. 559–568, 2015, doi: 10.1016/j.carbpol.2014.10.009.
79. S. Roy and J. W. Rhim, "Carboxymethyl cellulose-based antioxidant and antimicrobial active packaging film incorporated with curcumin and zinc oxide," Int. J. Biol. Macromol., vol. 148, pp. 666–676, 2020, doi: 10.1016/j.ijbiomac.2020.01.204.
80. J. I. Kadokawa, T. Arimura, Y. Takemoto, and K. Yamamoto, "Self-assembly of amylose-grafted carboxymethyl cellulose," Carbohydr. Polym., vol. 90, no. 3, pp. 1371–1377, 2012, doi: 10.1016/j.carbpol.2012.07.006.
81. M. Ali, N. R. Khan, H. M. Basit, and S. Mahmood, "Physico-chemical based mechanistic insight into surfactant modulated sodium Carboxymethylcellulose film for skin tissue regeneration applications," J. Polym. Res., vol. 27, no. 1, 2020, doi: 10.1007/s10965-019-1987-y.
82. M. Easson, A. Villalpando, and B. D. Condon, "Absorbent properties of carboxymethylated fiber, hydroentangled nonwoven and regenerated cellulose: A comparative study," J. Eng. Fiber. Fabr., vol. 12, no. 4, pp. 61–69, 2017, doi: 10.1177/155892501701200408.
83. X. H. Yang and W. L. Zhu, "Viscosity properties of sodium carboxymethylcellulose solutions," Cellulose, vol. 14, no. 5, pp. 409–417, 2007, doi: 10.1007/s10570-007-9137-9.
84. P. E. Napoli, F. Coronella, G. M. Satta, I. A. Zucca, and M. Fossarello, "A novel OCT technique to measure in vivo the corneal adhesiveness for sodium carboxymethylcellulose in humans and its validity in the diagnosis of dry eye," Investig. Ophthalmol. Vis. Sci., vol. 55, no. 5, pp. 3179–3185, 2014, doi: 10.1167/iovs.13-13613.
85. B. N. Singh, N. N. Panda, R. Mund, and K. Pramanik, "Carboxymethyl cellulose enables silk fibroin nanofibrous scaffold with enhanced biomimetic potential for bone tissue engineering application," Carbohydr. Polym., vol. 151, pp. 335–347, 2016, doi: 10.1016/j.carbpol.2016.05.088.
86. T. Mohan et al., "Generic Method for Designing Self-Standing and Dual Porous 3D Bioscaffolds from Cellulosic Nanomaterials for Tissue Engineering Applications," ACS Appl. Bio Mater., vol. 3, no. 2, pp. 1197–1209, 2020, doi: 10.1021/acsabm.9b01099.

87. S. Sadeghi, J. Nourmohammadi, A. Ghaee, and N. Soleimani, “Carboxymethyl cellulose-human hair keratin hydrogel with controlled clindamycin release as antibacterial wound dressing,” Int. J. Biol. Macromol., vol. 147, pp. 1239–1247, 2020, doi: 10.1016/j.ijbiomac.2019.09.251.
88. N. A. Dahlan, J. Pushpamalar, A. K. Veeramachineni, and S. Muniyandy, “Smart Hydrogel of Carboxymethyl Cellulose Grafted Carboxymethyl Polyvinyl Alcohol and Properties Studied for Future Material Applications,” J. Polym. Environ., vol. 26, no. 5, pp. 2061–2071, 2018, doi: 10.1007/s10924-017-1105-3.
89. N. Roy, N. Saha, T. Kitano, and P. Saha, “Biodegradation of PVP-CMC hydrogel film: A useful food packaging material,” Carbohydr. Polym., vol. 89, no. 2, pp. 346–353, 2012, doi: 10.1016/j.carbpol.2012.03.008.
90. A. Khezrian and Y. Shahbazi, “Application of nanocompostie chitosan and carboxymethyl cellulose films containing natural preservative compounds in minced camel’s meat,” Int. J. Biol. Macromol., vol. 106, pp. 1146–1158, 2018, doi: 10.1016/j.ijbiomac.2017.08.117.
91. H. F. Youssef, M. E. El-Naggar, F. K. Fouda, and A. M. Youssef, “Antimicrobial packaging film based on biodegradable CMC/PVA-zeolite doped with noble metal cations,” Food Packag. Shelf Life, vol. 22, no. July, p. 100378, 2019, doi: 10.1016/j.fpsl.2019.100378.
92. H. Guo et al., “Intelligent carboxymethyl cellulose composite films containing Garcinia mangostana shell anthocyanin with improved antioxidant and antibacterial properties,” Int. J. Biol. Macromol., vol. 263, no. P2, p. 130362, 2024, doi: 10.1016/j.ijbiomac.2024.130362.
93. A. Olatunde, A. Mohammed, M. A. Ibrahim, N. Tajuddeen, and M. N. Shuaibu, “Vanillin: A food additive with multiple biological activities,” Eur. J. Med. Chem. Reports, vol. 5, no. May, p. 100055, 2022, doi: 10.1016/j.ejmcr.2022.100055.
94. H. P. S. Makkar and K. Becker, “Isolation of Tannins from Leaves of Some Trees and Shrubs and Their Properties,” J. Agric. Food Chem., vol. 42, no. 3, pp. 731–734, 1994, doi: 10.1021/jf00039a026.
95. N. J. Walton, M. J. Mayer, and A. Narbad, “Vanillin,” Phytochemistry, vol. 63, no. 5, pp. 505–515, 2003, doi: 10.1016/S0031-9422(03)00149-3.
96. L. Xu, F. Liaqat, J. Sun, M. I. Khazi, R. Xie, and D. Zhu, “Advances in the vanillin synthesis and biotransformation: A review,” Renew. Sustain. Energy Rev., vol. 189, no. PA, p. 113905, 2024, doi: 10.1016/j.rser.2023.113905.
97. G. Banerjee and P. Chattopadhyay, “Vanillin biotechnology: the perspectives and future,” J. Sci. Food Agric., vol. 99, no. 2, pp. 499–506, 2019, doi: 10.1002/jsfa.9303.
98. G. Bettio, L. C. Zardo, C. A. Rosa, and M. A. Záchia Ayub, “Bioconversion of ferulic acid into aroma compounds by newly isolated yeast strains of the Latin American biodiversity,” Biotechnol. Prog., vol. 37, no. 1, pp. 1–15, 2021, doi: 10.1002/btpr.3067.
99. G. A. Martău, L. F. Călinoiu, and D. C. Vodnar, “Bio-vanillin: Towards a sustainable industrial production,” Trends Food Sci. Technol., vol. 109, no. October 2020, pp. 579–592, 2021, doi: 10.1016/j.tifs.2021.01.059.
100. T. Furuya, M. Kuroiwa, and K. Kino, “Biotechnological production of vanillin

using immobilized enzymes," J. Biotechnol., vol. 243, pp. 25–28, 2017, doi: 10.1016/j.jbiotec.2016.12.021.
101. H. et al. Galadima, A.I., Salleh, M.M., Hussin, "Biovanillin: production concepts and prevention of side product formation," Biomass Convers. Biorefinery, vol. 10, no. 2020, pp. 589–609, 2019, [Online]. Available: https://doi.org/10.1007/s13399-019-00418-0
102. B. Kaur and D. Chakraborty, "Biotechnological and molecular approaches for vanillin production: A review," Appl. Biochem. Biotechnol., vol. 169, no. 4, pp. 1353–1372, 2013, doi: 10.1007/s12010-012-0066-1.
103. I. Ibrar, L. Alsaka, S. Yadav, A. Altaee, J. L. Zhou, and H. K. Shon, "Kappa carrageenan-vanillin composite hydrogel for landfill leachate wastewater treatment," Desalination, vol. 565, no. May, p. 116826, 2023, doi: 10.1016/j.desal.2023.116826.
104. F. Liaqat, L. Xu, M. I. Khazi, S. Ali, M. U. Rahman, and D. Zhu, "Extraction, purification, and applications of vanillin: A review of recent advances and challenges," Ind. Crops Prod., vol. 204, no. PB, p. 117372, 2023, doi: 10.1016/j.indcrop.2023.117372.
105. J. Hu et al., "Vanillin-bioglass cross-linked 3D porous chitosan scaffolds with strong osteopromotive and antibacterial abilities for bone tissue engineering," Carbohydr. Polym., vol. 271, no. July, p. 118440, 2021, doi: 10.1016/j.carbpol.2021.118440.
106. I. Negut, G. Dorcioman, and V. Grumezescu, "Sca ff olds for Wound Healing Applications," 2020.
107. G. Zhou et al., "Research on a novel poly (vinyl alcohol)/lysine/vanillin wound dressing: Biocompatibility, bioactivity and antimicrobial activity," Burns, vol. 40, no. 8, pp. 1668–1678, 2014, doi: 10.1016/j.burns.2014.04.005.
108. H. Yu, Y. Ge, H. Ding, Y. Yan, and L. Wang, "Vanillin cross-linked chitosan/gelatin bio-polymer film with antioxidant, water resistance and ultraviolet-proof properties," Int. J. Biol. Macromol., vol. 253, no. P2, p. 126726, 2023, doi: 10.1016/j.ijbiomac.2023.126726.
109. B. Tomadoni, A. Ponce, M. Pereda, and M. R. Ansorena, "Vanillin as a natural cross-linking agent in chitosan-based films: Optimizing formulation by response surface methodology," Polym. Test., vol. 78, no. May, p. 105935, 2019, doi: 10.1016/j.polymertesting.2019.105935.
110. A. Sharma, S. Sahu, S. Sharma, G. Singh, and S. K. Arya, "Valorization of agro-industrial wastes into vanillin: A sustainable and bio-economical step towards the indigenous production of flavors," Biocatal. Agric. Biotechnol., vol. 54, no. October, p. 102904, 2023, doi: 10.1016/j.bcab.2023.102904.
111. S. Gomathi and M. Rameshpathy, "Valorization of agro-waste residues into bio-vanillin a comprehensive review," Ind. Crops Prod., vol. 205, no. March, p. 117522, 2023, doi: 10.1016/j.indcrop.2023.117522.
112. V. Paul, N. Rai, A. Agarwal, V. Gautam, and A. D. Tripathi, "Valorization of lignocellulosic waste (coconut coir) for bio-vanillin production having antioxidant and anticancer activity against human breast cancer cells (MCF-7)," Ind. Crops Prod., vol. 205, no. August, p. 117502, 2023, doi:

10.1016/j.indcrop.2023.117502.
113. H. H. Murray, Applied Clay Mineralogy: Occurrences, Processing and Application of Kaolins, Bentonites, Palygorskite-Sepiolite, and Common Clays, vol. 2. Elsevier, 2007. [Online]. Available: http://www.sciencedirect.com/science/article/pii/S1572435206020010
114. S. Pavlidou and C. D. Papaspyrides, "A review on polymer-layered silicate nanocomposites," Prog. Polym. Sci., vol. 33, no. 12, pp. 1119–1198, 2008, doi: 10.1016/j.progpolymsci.2008.07.008.
115. M. L. Gualtieri, A. F. Gualtieri, S. Gagliardi, P. Ruffini, R. Ferrari, and M. Hanuskova, "Thermal conductivity of fired clays: Effects of mineralogical and physical properties of the raw materials," Appl. Clay Sci., vol. 49, no. 3, pp. 269–275, 2010, doi: 10.1016/j.clay.2010.06.002.
116. D. Nath, S. R, K. Pal, and P. Sarkar, "Nanoclay-based active food packaging systems: A review," Food Packag. Shelf Life, vol. 31, no. May 2021, p. 100803, 2022, doi: 10.1016/j.fpsl.2021.100803.
117. N. Farzadnia, A. A. Abang Ali, R. Demirboga, and M. P. Anwar, "Effect of halloysite nanoclay on mechanical properties, thermal behavior and microstructure of cement mortars," Cem. Concr. Res., vol. 48, pp. 97–104, 2013, doi: 10.1016/j.cemconres.2013.03.005.
118. M. Alexandre and P. Dubois, "Polymer-layered silicate nanocomposites: Preparation, properties and uses of a new class of materials," Mater. Sci. Eng. R Reports, vol. 28, no. 1, pp. 1–63, 2000, doi: 10.1016/S0927-796X(00)00012-7.
119. J. W. Cho and D. R. Paul, "Nylon 6 nanocomposites by melt compounding," Polymer (Guildf)., vol. 42, no. 3, pp. 1083–1094, 2001, doi: 10.1016/S0032-3861(00)00380-3.
120. E. M. C. Alexandre, R. V. Lourenço, A. M. Q. B. Bittante, I. C. F. Moraes, and P. J. do A. Sobral, "Gelatin-based films reinforced with montmorillonite and activated with nanoemulsion of ginger essential oil for food packaging applications," Food Packag. Shelf Life, vol. 10, pp. 87–96, 2016, doi: 10.1016/j.fpsl.2016.10.004.
121. K. Varlot, E. Reynaud, M. H. Kloppfer, G. Vigier, and J. Varlet, "Clay-reinforced polyamide: Preferential orientation of the montmorillonite sheets and the polyamide crystalline lamellae," J. Polym. Sci. Part B Polym. Phys., vol. 39, no. 12, pp. 1360–1370, 2001, doi: 10.1002/POLB.1108.
122. H. Onyeaka, P. Passaretti, T. Miri, and Z. T. Al-Sharify, "The safety of nanomaterials in food production and packaging," Curr. Res. Food Sci., vol. 5, no. October 2021, pp. 763–774, 2022, doi: 10.1016/j.crfs.2022.04.005.
123. J. R. A. Pires, V. G. L. de Souza, and A. L. Fernando, "Chitosan/montmorillonite bionanocomposites incorporated with rosemary and ginger essential oil as packaging for fresh poultry meat," Food Packag. Shelf Life, vol. 17, no. July, pp. 142–149, 2018, doi: 10.1016/j.fpsl.2018.06.011.
124. S. M. Lee and D. Tiwari, "Organo and inorgano-organo-modified clays in the remediation of aqueous solutions: An overview," Appl. Clay Sci., vol. 59–60, pp. 84–102, 2012, doi: 10.1016/j.clay.2012.02.006.
125. R. Rafiee and R. Shahzadi, "Mechanical Properties of Nanoclay and Nanoclay

Reinforced Polymers: A Review," Polym. Compos., vol. 40, no. 2, pp. 431–445, 2019, doi: 10.1002/PC.24725.
126. N. P. Risyon, S. H. Othman, R. K. Basha, and R. A. Talib, "Characterization of polylactic acid/halloysite nanotubes bionanocomposite films for food packaging," Food Packag. Shelf Life, vol. 23, no. December 2019, p. 100450, 2020, doi: 10.1016/j.fpsl.2019.100450.
127. A. Wagner et al., "Toxicity evaluations of nanoclays and thermally degraded byproducts through spectroscopical and microscopical approaches," Biochim. Biophys. Acta - Gen. Subj., vol. 1861, no. 1, pp. 3406–3415, 2017, doi: 10.1016/j.bbagen.2016.09.003.
128. S. Jayrajsinh, G. Shankar, Y. K. Agrawal, and L. Bakre, "Montmorillonite nanoclay as a multifaceted drug-delivery carrier: A review," J. Drug Deliv. Sci. Technol., vol. 39, pp. 200–209, 2017, doi: 10.1016/j.jddst.2017.03.023.
129. J. H. Hassen, H. K. Abdalkadir, and S. F. Abed, "An overview of medical applications of montmorillonite clay," J. Med. Sci., vol. 92, no. 2, p. e826, 2023, doi: 10.20883/medical.e826.
130. M. Wu et al., "Nanoclay mineral-reinforced macroporous nanocomposite scaffolds for in situ bone regeneration: In vitro and in vivo studies," Mater. Des., vol. 205, p. 109734, 2021, doi: 10.1016/j.matdes.2021.109734.
131. S. I. Hossain et al., "A Review on Montmorillonite-Based Nanoantimicrobials: State of the Art," Nanomaterials, vol. 13, no. 5, pp. 1–34, 2023, doi: 10.3390/nano13050848.
132. P. R. Oliveira-Pinto et al., "Montmorillonite Nanoclay and Formulation with Satureja montana Essential Oil as a Tool to Alleviate Xanthomonas euvesicatoria Load on Solanum lycopersicum," Appl. Nano, vol. 3, no. 3, pp. 126–142, 2022, doi: 10.3390/applnano3030009.
133. S. Lordan, J. E. Kennedy, and C. L. Higginbotham, "Cytotoxic effects induced by unmodified and organically modified nanoclays in the human hepatic HepG2 cell line," J. Appl. Toxicol., vol. 31, no. 1, pp. 27–35, 2011, doi: 10.1002/JAT.1564.
134. S. Maisanaba et al., "Toxic effects of a modified montmorillonite clay on the human intestinal cell line Caco-2," J. Appl. Toxicol., vol. 34, no. 6, pp. 714–725, 2014, doi: 10.1002/JAT.2945.
135. S. Maisanaba, K. Hercog, M. Filipic, Á. Jos, and B. Zegura, "Genotoxic potential of montmorillonite clay mineral and alteration in the expression of genes involved in toxicity mechanisms in the human hepatoma cell line HepG2," J. Hazard. Mater., vol. 304, pp. 425–433, 2016, doi: 10.1016/j.jhazmat.2015.10.018.
136. A. K. Sharma, B. Schmidt, H. Frandsen, N. R. Jacobsen, E. H. Larsen, and M. L. Binderup, "Genotoxicity of unmodified and organo-modified montmorillonite," Mutat. Res. - Genet. Toxicol. Environ. Mutagen., vol. 700, no. 1–2, pp. 18–25, 2010, doi: 10.1016/j.mrgentox.2010.04.021.
137. P. R. Li, J. C. Wei, Y. F. Chiu, H. L. Su, F. C. Peng, and J. J. Lin, "Evaluation on cytotoxicity and genotoxicity of the exfoliated silicate nanoclay," ACS Appl. Mater. Interfaces, vol. 2, no. 6, pp. 1608–1613, 2010, doi: 10.1021/am1001162.
138. M. Baek, J. A. Lee, and S. J. Choi, "Toxicological effects of a cationic clay, montmorillonite in vitro and in vivo," Mol. Cell. Toxicol., vol. 8, no. 1, pp. 95–

101, 2012, doi: 10.1007/s13273-012-0012-x.
139. "Inventory of Effective Food Contact Substance (FCS) Notifications | FDA." [Online]. Available: https://www.fda.gov/food/packaging-food-contact-substances-fcs/inventory-effective-food-contact-substance-fcs-notifications
140. "EFSA Journal - 2015 - - Safety assessment of the substance montmorillonite clay modified by dimethyldialkyl C16-C18.pdf."
141. K. Y. Perera, M. Hopkins, A. K. Jaiswal, and S. Jaiswal, "Nanoclays-containing bio-based packaging materials: properties, applications, safety, and regulatory issues," J. Nanostructure Chem., vol. 14, no. 1, pp. 71–93, 2024, doi: 10.1007/s40097-023-00525-5.
142. N. Bumbudsanpharoke and S. Ko, "Nanoclays in food and beverage packaging," J. Nanomater., vol. 2019, 2019, doi: 10.1155/2019/8927167.
143. A. E. Giannakas and A. A. Leontiou, "Montmorillonite Composite Materials and Food Packaging," Compos. Mater. Food Packag., pp. 1–71, 2017, doi: 10.1002/9781119160243.CH1.
144. K. Król-Morkisz and K. Pielichowska, "Thermal Decomposition of Polymer Nanocomposites With Functionalized Nanoparticles," Polym. Compos. with Funct. Nanoparticles Synth. Prop. Appl., pp. 405–435, 2019, doi: 10.1016/B978-0-12-814064-2.00013-5.
145. E. Jamróz, P. Kulawik, and P. Kopel, "The effect of nanofillers on the functional properties of biopolymer-based films: A review," Polymers (Basel)., vol. 11, no. 4, pp. 1–43, 2019, doi: 10.3390/polym11040675.
146. J. F. Martucci and R. A. Ruseckaite, "Antibacterial activity of gelatin/copper (II)-exchanged montmorillonite films," Food Hydrocoll., vol. 64, pp. 70–77, 2017, doi: 10.1016/j.foodhyd.2016.10.030.
147. F. Rodriguez, H. M. Sepulveda, J. Bruna, A. Guarda, and M. J. Galotto, "Development of Cellulose Eco-nanocomposites with Antimicrobial Properties Oriented for Food Packaging," Packag. Technol. Sci., vol. 26, no. 3, pp. 149–160, Apr. 2013, doi: 10.1002/PTS.1980.
148. H. M. Park, M. Misra, L. T. Drzal, and A. K. Mohanty, "'Green' nanocomposites from cellulose acetate bioplastic and clay: Effect of eco-friendly triethyl citrate plasticizer," Biomacromolecules, vol. 5, no. 6, pp. 2281–2288, 2004, doi: 10.1021/bm049690f.
149. F. J. Rodríguez, A. Coloma, M. J. Galotto, A. Guarda, and J. E. Bruna, "Effect of organoclay content and molecular weight on cellulose acetate nanocomposites properties," Polym. Degrad. Stab., vol. 97, no. 10, pp. 1996–2001, 2012, doi: 10.1016/j.polymdegradstab.2012.06.003.
150. F. J. Rodríguez, M. J. Galotto, A. Guarda, and J. E. Bruna, "Modification of cellulose acetate films using nanofillers based on organoclays," J. Food Eng., vol. 110, no. 2, pp. 262–268, 2012, doi: 10.1016/j.jfoodeng.2011.05.004.
151. V. G. L. Souza et al., "Bionanocomposites of chitosan/montmorillonite incorporated with Rosmarinus officinalis essential oil: Development and physical characterization," Food Packag. Shelf Life, vol. 16, no. March, pp. 148–156, 2018, doi: 10.1016/j.fpsl.2018.03.009.
152. M. Lavorgna et al., "MMT-supported Ag nanoparticles for chitosan

nanocomposites: Structural properties and antibacterial activity," Carbohydr. Polym., vol. 102, no. 1, pp. 385–392, 2014, doi: 10.1016/j.carbpol.2013.11.026.
153. H. Li, H. Shi, Y. He, X. Fei, and L. Peng, "Preparation and characterization of carboxymethyl cellulose-based composite films reinforced by cellulose nanocrystals derived from pea hull waste for food packaging applications," Int. J. Biol. Macromol., vol. 164, pp. 4104–4112, 2020, doi: 10.1016/j.ijbiomac.2020.09.010.
154. P. Jha, "Effect of plasticizer and antimicrobial agents on functional properties of bionanocomposite films based on corn starch-chitosan for food packaging applications," Int. J. Biol. Macromol., vol. 160, pp. 571–582, 2020, doi: 10.1016/j.ijbiomac.2020.05.242.
155. Z. H. Zhang, Z. Han, X. A. Zeng, X. Y. Xiong, and Y. J. Liu, "Enhancing mechanical properties of chitosan films via modification with vanillin," Int. J. Biol. Macromol., vol. 81, pp. 638–643, 2015, doi: 10.1016/j.ijbiomac.2015.08.042.
156. L. A. Sarabia and M. C. Ortiz, "Response Surface Methodology," Compr. Chemom., vol. 1, pp. 345–390, 2009, doi: 10.1016/B978-044452701-1.00083-1.
157. Y. Zahedi, B. Fathi-Achachlouei, and A. R. Yousefi, "Physical and mechanical properties of hybrid montmorillonite/zinc oxide reinforced carboxymethyl cellulose nanocomposites," Int. J. Biol. Macromol., vol. 108, pp. 863–873, 2018, doi: 10.1016/j.ijbiomac.2017.10.185.
158. D. B. Williams and C. B. Carter, Transmission Electron Microscopy. 2009. doi: 10.1007/978-981-19-3509-1_4.
159. M. De Graef, "Introduction to Conventional Transmission Electron Microscopy," Mater. Today, vol. 6, no. 6, p. 57, 2003, doi: 10.1016/S1369-7021(03)00636-9.
160. E. J. Kirkland, Advanced Computing in Electron Microscopy. 2010. doi: 10.1046/j.1365-2818.1999.0550b.x.
161. H. M. Cele et al., "Effect of nanoclay on optical properties of PLA/clay composite films," Polym. Test., vol. 36, no. 2014, pp. 24–31, 2014, doi: 10.1016/j.polymertesting.2014.03.010.
162. N. J. Venkatesha, B. S. Jai Prakash, and Y. S. Bhat, "The active site accessibility aspect of montmorillonite for ketone yield in ester rearrangement," Catal. Sci. Technol., vol. 5, no. 3, pp. 1629–1637, 2015, doi: 10.1039/c4cy01356e.
163. S. Lamidi, N. Olaleye, Y. Bankole, A. Obalola, E. Aribike, and I. Adigun, Applications of Response Surface Methodology (RSM) in Product Design, Development, and Process Optimization. 2023. doi: DOI: http://dx.doi.org/10.5772/intechopen.106763.
164. M. Hemavathi et al., "Robustness of sequential third-order response surface design to missing observations," J. Taibah Univ. Sci., vol. 16, no. 1, pp. 270–279, 2022, doi: 10.1080/16583655.2022.2046398.
165. K. M. Carley, N. Y. Kamneva, and J. Reminga, "Response Surface Methodology," 2004. [Online]. Available: http://www.casos.cs.cmu.edu/publications/papers/CMU-ISR-04-136.pdf

Appendix

Appendix A: Energy Dispersive Spectrum of the Nanoclay Area

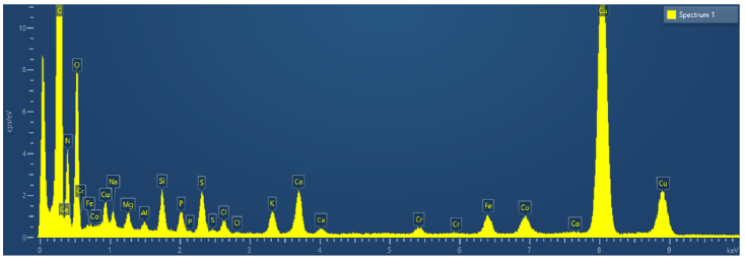

Figure 14: EDS Spectrum Showing the Peaks from Nanoclay (Except Cu, Cr, Fe, and Co)

Appendix B: Energy Dispersive Spectrum Maps of the Nanoclay Area

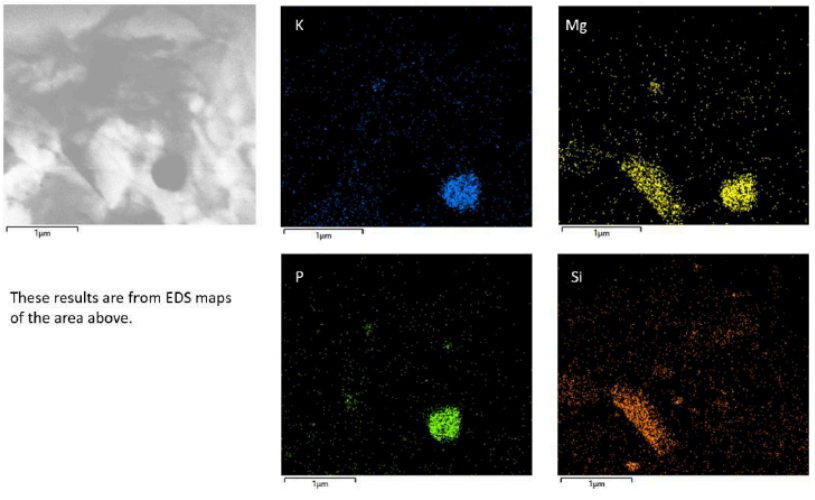

Figure 15: EDS Maps

Appendix C: Prototype of CMC/Vanillin/MMT nanoclay

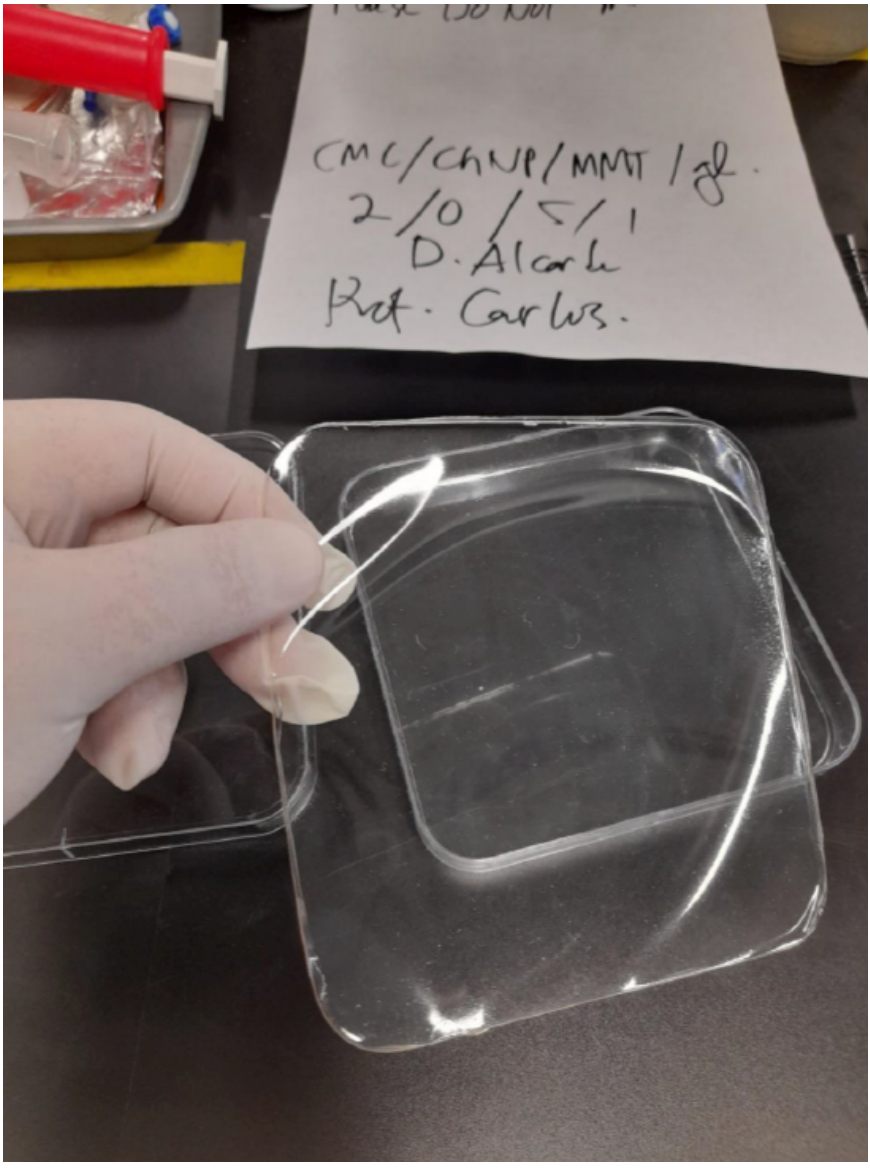

Figure 16: Prototype of CMC/Vanillin/MMT nanoclay